Journal of Ecohumanism
2024
Volume: 3, No: 8, pp. 2207 – 2234
ISSN: 2752-6798 (Print) | ISSN 2752-6801 (Online)
https://ecohumanism.co.uk/joe/ecohumanism
DOI: https://doi.org/10.62754/joe.v3i8.4898

Estimation of Future Climate Change in Low Folded Zone, Iraq with the LARS-WG and Five GMS Models under CMIP5 Scenarios

Noor Q.Sabri[1], Thair S. Khayyun[2]

Abstract

This study investigates the trends of climate change in the Low Folded Zone region of Iraq and provides future projections for daily maximum and minimum temperatures, as well as precipitation. Using the LARS-WG model and five General Circulation Models (GCMs) under three Representative Concentration Pathways (RCP) scenarios, the research aims to provide valuable insights into the anticipated changes in climate variables. The calibration and validation of the model demonstrate its capability to simulate future climatic data, with statistical indices indicating a strong correlation between observed and generated data. The projected future temperatures showed a consistent increase across all selected stations, with average annual maximum temperatures expected to rise by 1.06 to 5.48°C by the end of the twenty-first century. The highest increase in temperatures was predicted under the high-emission scenario RCP8.5. The results also indicated spatial and temporal variations in precipitation patterns, with the annual percentage increase in precipitation ranging from 7.07% to 10.75% for RCP 2.6, 0% to 2.2% for RCP4.5, and 3.7% to 6.8% for RCP8.5. The findings reveal a projected increase in annual temperatures and variable precipitation patterns, highlighting the urgency of proactive measures to address the challenges posed by climate change in the region. The results of this study are crucial for informing decision-makers and planners in developing strategies for climate change adaptation and resource management, particularly in water resource management and agricultural planning.

Keywords: *Climate Change, Gcms, Downscaling, LARS-WG, Precipitation, Temperatures.*

Introduction

The Middle East is a region highly susceptible to climate change impacts due to its arid and semi-arid landscapes. The climate change consequences have already taken place in some countries such as Turkey, Iran, Iraq, Kuwait, Saudi Arabia, Qatar, Sudan, and Syria [1- 4]. Climate change affects both the environment and human systems, leading to risks such as heat stress, storms, flooding, water scarcity, and threats to agriculture and food security [5-8]. The primary cause of climate change is the increase in greenhouse gas emissions, predominantly driven by economic and population growth. This has resulted in unprecedented levels of methane (CH4), carbon dioxide (CO2), and nitrous oxide (N2O) in the atmosphere [9-11].

To assess climate risks and understand future climate projections, scientists commonly utilize global climate models (GCMs) [13-15]. which are powerful tools for modeling the three-dimensional climate system utilizing equations defining energy (first law of thermodynamics), momentum (Newton's second law of motion), conservation of mass (continuity equation), and water vapor (ideal gas law). Each equation is calculated for distinct layers of the atmosphere that are delineated by a regular grid at discrete locations on the Earth's surface, during predetermined periods of time [16, 17]. However, GCMs have limitations due to their coarse spatial resolution and inability to capture regional-scale phenomena [18]. To address this, researchers employ downscaling methods that bridge the gap between GCM outputs and finer-scale climate data [19,20]. These methods include dynamical downscaling using Regional Climate Models (RCMs) and statistical downscaling models such as the LARS-WG and statistical downscaling models SDSM [21,22].

Iraq is a country significantly affected by climate change, with diverse climates across its regions [23]. The nation's heavy reliance on oil production has contributed to increased carbon dioxide emissions, exacerbating the impacts of climate change [24]. Furthermore, the construction of dams by neighboring

[1] Civil Engineering Department, University of Technology, Baghdad-Iraq, Email: bce.19.86@grad.uotechnology.edu.iq, (Corresponding Author)
[2] Civil Engineering Department, University of Technology, Baghdad-Iraq, Email: 40073@uotechnology.edu.iq.

Journal of Ecohumanism
2024
Volume: 3, No: 8, pp. 2207 – 2234
ISSN: 2752-6798 (Print) | ISSN 2752-6801 (Online)
https://ecohumanism.co.uk/joe/ecohumanism
DOI: https://doi.org/10.62754/joe.v3i8.4898

countries, including Syria, Iran, and Turkey, has reduced river flow, water scarcity, land degradation, and desertification within Iraq [25].

In addition to these challenges, inadequate water management practices and outdated agricultural techniques further contribute to water scarcity in Iraq. The agricultural sector consumes a significant portion of the available freshwater, intensifying the strain on water resources [26-28]. These factors have amplified the impacts of climate change on Iraq, posing significant socioeconomic and environmental challenges.

This study aims to investigate climate change trends and future projections in Iraq, specifically focusing on the Low Folded Zone region. By employing advanced modeling techniques, such as the LARS-WG model and GCMs, the research aims to provide valuable insights into the anticipated changes in temperature and precipitation patterns within the region. The findings of this study will contribute to a better understanding of the magnitude of climate change impacts in the Low Folded Zone and support the development of effective strategies for adaptation and mitigation. Additionally, the research will inform water and agricultural resource management, promoting sustainable practices and enhancing resilience in the face of climate change.

Material and Methods

Study Area Description

The Low Folded Zone comprises a significant portion, specifically 13.6%, of Iraq's total geographical area, covering a vast expanse measuring 56930 square kilometres. The region's geographical position is in Iraq's north and northwest central regions, as illustrated in Figure 1a. The topography of this region exhibits a gradual elevation gradient, commencing from the southwestern boundary at an elevation range of 125 to 300 meters above mean sea level and progressively ascending toward the northern and eastern perimeters, where it attains altitudes that range from 900 to one thousand meters above mean sea level. The geographical area being examined includes several notable aquifers, specifically the Fatha, Injana, Mukdadiyah, Bai Hassan Constructions, and Quaternary deposits. The Low Folded Zone consists of thirteen sub-provinces,

The study area is divided into 13 hydrogeological Sub provinces, namely: Erbil, Dohuk – Alqosh, West Tigris River, Sinjar – Rabee'a, Khazir – Gomel, Altun Kupri, Dibiga, Makhmour, Kirkuk – Hawija – Tuz Khurmatu, Cham Chamal – Qadir Karam – Qara Too, Kalar – Khanaqeen, Qara Tappa – Al-Sa'adiyah and Mandili – Zurbatiya – Teeb [29].

Journal of Ecohumanism
2024
Volume: 3, No: 8, pp. 2207 – 2234
ISSN: 2752-6798 (Print) | ISSN 2752-6801 (Online)
https://ecohumanism.co.uk/joe/ecohumanism
DOI: https://doi.org/10.62754/joe.v3i8.4898

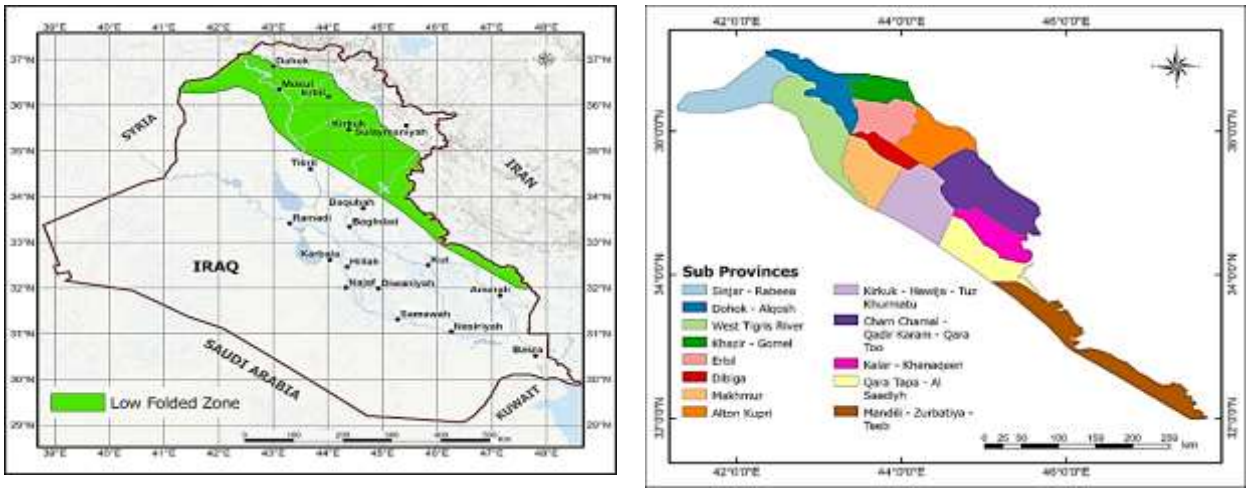

Figure 1. Location And Sub-Provinces Maps of The Study Area.

Table 1. Coordinates and Elevations of the Selected Stations.

Station	Latitude	Longitude	Elevation (m)	Period of record
Sinjar - Rabeea	36º 34´ 51˝ N	42º 2´ 52˝ E	865	1990-2020
Dohok - Alqosh	36º 38´ 10˝ N	43º 3´ 30˝ E	580	1990-2020
West Tigris River	36º 3´ 51˝ N	42º 58´ 46˝ E	360	1990-2020
Khazir - Gomel	36º 34´ 51˝ N	43º 44´ 14˝ E	1085	1990-2020
Erbil	36º 10´ 11˝ N	43º 48´ 34˝ E	465	1990-2020
Dibiga	35º 43´ 55˝ N	43º 50´ 18˝ E	470	1990-2020
Makhmur	35º26´ 20˝ N	43º 36´ 2˝ E	450	1990-2020
Alton Kupri	35º 52´ 19˝ N	44º 23´ 33˝ E	750	1990-2020
Kirkuk - Hawija - Tuz Khurmatu	35º 0´ 19˝ N	44º 12´ 43˝ E	250	1990-2020
Cham Chamal - Qadir Karam	35º 8´ 35˝ N	45º 0´ 48˝ E	1007	1990-2020
Kalar - Khanaqeen	34º 32´ 39˝ N	45º 8´ 41˝ E	231	1990-2020
Qara Tapa - Al Saadiyh	34º 16´ 56˝ N	44º 57´ 37˝ E	333	1990-2020
Mandili - Zurbatiya - Teeb	32º 52´ 26˝ N	46º 21´ 12˝ E	512	1990-2020

meteorological database for Climate Forecast System Reanalysis (CFSR) for the period January 1990 to December 2014 (https:// swat. tamu. edu/ data/ cfsr). The additional daily Temperature data were obtained from ERA5-Land monthly averaged data from 2015 to 2020 [30]. The additional daily Precipitation data was obtained from [31] averaged data from 2015 to 2020

LARS-WG Model

Global Climate Models (GCMs) are often used to simulate current and future climate conditions. However, due to their coarse spatial resolution and inability to capture regional-scale phenomena, researchers commonly employ downscaling methods to bridge the gap between GCM outputs and finer-scale climate data. One widely used downscaling tool is the Long Ashton Research Station Weather Generator (LARS-WG) [32], a statistical model that offers flexibility, computational efficiency, and simplicity in simulating weather data LARS-WG enables the generation of daily time series for various climate variables, including precipitation, maximum and minimum temperatures, and solar radiation [33,34]. The model employs a semi-empirical distribution to approximate the probability distributions of wet and dry series, daily Precipitation, and temperatures. Using LARS-WG, researchers can generate synthetic weather data for

Journal of Ecohumanism
2024
Volume: 3, No: 8, pp. 2207 – 2234
ISSN: 2752-6798 (Print) | ISSN 2752-6801 (Online)
https://ecohumanism.co.uk/joe/ecohumanism
DOI: https://doi.org/10.62754/joe.v3i8.4898

present and future climate events based on historical data obtained from GCMs. This approach allows for a more detailed and localized understanding of climate change impacts, particularly in arid and semi-arid regions like Iraq.

The following Equation determines the value v_i of a climate variable v corresponding to a given probability p_i for each variable.

$$v_i = min\{v : p\ (v_{obs} \leq v) \geq p_i\}: \qquad i = 0, \ldots, n \qquad (1)$$

where P ($v_{obs} \leq$ v) represents the probability depending on v_{obs} , the observed data. Two values, P_o and P_n , remain constant as $P_o = 0$ and $P_n = 1$, respectively, with according values for v_o = min v_{obs} and v_n = max v_{obs}, depending on v_{obs}

Global Climate Model (GCMs)

GCMs serve as essential tools for projecting future climate conditions by simulating the Earth's climate system. to estimate future climate change, five GCMs from the Coupled Model Intercomparison Project Phase 5 (CMIP5) were utilized. These GCMs are widely recognized for their comprehensive representation of the atmosphere, ocean, land surface, and sea ice interactions based on the underlying physical and mathematical principles. The selected GCMs offer a diverse range of climate projections, allowing for a robust assessment of potential future climate scenarios. The models used in this study are presented in Table 2. Each of these GCMs provides valuable insights into the potential changes in temperature, precipitation, and other climate variables, enabling a comprehensive analysis of the future climate conditions in the study area. To generate future climate projections, the GCM outputs were downscaled to a regional scale using the Long Ashton Research Station Weather Generator (LARS-WG). The LARS-WG software is widely employed for downscaling GCM outputs, incorporating statistical relationships between large-scale climate variables and local weather patterns. By employing LARS-WG, we were able to obtain high-resolution climate data that are more suitable for local-scale analysis in the Low-Folded Zone of Iraq. The Representative Concentration Pathways (RCPs) used are 2.6, 4.5, and 8.5. These scenarios represent different greenhouse gas concentration trajectories and provide a range of possible future climate conditions. By considering multiple scenarios, we aimed to capture the uncertainty associated with future climate projections and assess the potential impacts of different emission pathways on the Low Folded Zone of Iraq.

In the context of climatic variables, specific P_i values are assigned to represent the lowest and highest values, ensuring an accurate portrayal of extreme climatic conditions. The remaining P_i values are evenly distributed across the probability range. For precipitation, three values near 1 p_{n-1} =0.999, p_{n-2} =0.995, and p_{n-3}= 0.985 are chosen to enable precise calculation of exceptionally rare high daily precipitation events. Additionally, to approximate precipitation within the range of 0 to 1, two values v_1= 0.5 mm and v_1= 1 mm are utilized, with corresponding probabilities calculated based on observed values. For the wet and dry series, values close to 1, p_{n-1} = 0.99 and p_{n-2} = 0.98 are employed to account for extended dry and wet periods. Similarly, values near 0 and 1 represent exceptionally high and low temperatures for maximum and minimum temperatures. This study utilized the latest version LARSWG 6, to model future climate change across three distinct periods: P1 (2040–2060), P2 (2060–2080), and P3 (2080–2100) relative to the reference period RP (1990–2020).

Table 2. The Selected Gcms Included in LARS-WG 6 and with RCP 2.6, RCP4.5 And RCP8.5 Scenarios

No.	GCM	Research center	RCP
1	BCC-CSM1	Beijing Climate Centre Institute of Atmospheric Physics	2.6, 4.5 , 8.5
2	CanESM2	The Canadian Earth System-second generation Model	2.6, 4.5 , 8.5
3	CSIRO-MK36	Australia's Commonwealth Scientific and Industrial Research Organization	2.6, 4.5 , 8.5
4	HadGEM2-ES	Hadley Centre Global Environment Model version 2	2.6, 4.5, 8.5
5	NorESM1	The Norwegian Earth System Model	2.6, 4.5 , 8.5

Journal of Ecohumanism
2024
Volume: 3, No: 8, pp. 2207 – 2234
ISSN: 2752-6798 (Print) | ISSN 2752-6801 (Online)
https://ecohumanism.co.uk/joe/ecohumanism
DOI: https://doi.org/10.62754/joe.v3i8.4898

Data Available and Modeling Procedures

Two observed weather data sets are required for each site to design weather generators for generating synthetic weather data. The first set should include daily values of minimum and maximum temperature, precipitation, and radiation or sunshine hours over a recommended 20 to 30 years. The second data set should be a (*.st) file containing station details such as name, longitude, latitude, altitude, and CO2 levels. Once these two files are prepared, the modeling procedures using LARS-WG can be initiated [33].

The modeling procedures involve two main steps:

Analysis

This step involves the analysis of observed data at a site, known as model calibration, to calculate site parameters. The resulting data is saved in three types of files:, (*.stx) file containing additional statistics, (*.wgx) file containing the site parameters, and (*.tst) file containing the statistical tests results.

Generator

Future weather data is generated to be comparable to observed data for each location in model validation. This process uses the (*.wgx) file to create a future scenario on a local scale. This process is done locally, corresponding to expected future climate changes derived from a global or local climate model.

Model Performance Indices

During the calibration and validation processes in LARS-WG, a (*.tst) file is generated, which contains the results of statistical tests comparing the synthetic weather data with the observed weather data. These tests evaluate the similarity between the two datasets and help assess the quality of the generated climate. The statistical tests performed include:

t-test for Monthly Means: This test compares the monthly means of the synthetic and observed weather data. It is conducted 12 times, once for each month. The t-test is computed using Equation (2).

f-test for Monthly Standard Deviations: This test compares the monthly standard deviations of the synthetic and observed weather data. It is also performed 12 times, corresponding to each month. The f-test is calculated using Equation (3).

Kolmogorov-Smirnov (K-S) Test for Daily Factors: The K-S test is utilized to compare the probability distributions of daily factors for each month at each location. This test is conducted 12 times, once each month. It assesses the similarity of the distributions and is represented by Equation (4).

Kolmogorov-Smirnov (K-S) Test for Seasonal Distribution: In this case, the K-S test is used to compare the distribution of the dry and wet series length throughout the seasons. This test is performed four times to cover all the seasons. The specific Equation used is not provided.

To determine the likelihood that the data occurred by chance under the assumption that the null hypothesis is correct, a p-value is computed for each test. If the p-value is very low, less than 0.01 or 0.05, it indicates that the generated climate is not similar to the observed. A p-value of 0.05 is commonly used as a significant level in statistical tests [35]. A perfect fit corresponds to a p-value of 1, a perfect fit is indicated by $0.7 \leq P < 1$, a good fit falls within the range of $0.4 \leq P < 0.7$, while a poor fit is represented by $P < 0.4$.

$$t = \frac{\bar{x}_1 - \bar{x}_2}{\sqrt{\frac{s_1^2}{n_1 - 1} - \frac{s_2^2}{n_2 - 1}}} \quad (2)$$

Journal of Ecohumanism
2024
Volume: 3, No: 8, pp. 2207 – 2234
ISSN: 2752-6798 (Print) | ISSN 2752-6801 (Online)
https://ecohumanism.co.uk/joe/ecohumanism
DOI: https://doi.org/10.62754/joe.v3i8.4898

where the : $\bar{x}_1, s_1^2$, $and\ n_1 - 1$ are the mean, standard deviations and the size of the observed dataset, respectively, while $\bar{x}_2, s_1^2\ and\ n_2 - 1$ are the mean, standard deviations and the size of the generated dataset, respectively.

$$f = \frac{S_1^2}{S_2^2} \quad (3)$$

where S_1^2 and $squared\ are$e the variance of the observed and generated data, respectively.

$$D = |Fn_1(x) - Fn_2(x)| \quad (4)$$

In this expression, $1\ represents$the collected information, whereas n_2 corresponds to the simulated data. To evaluate the effectiveness of the LARSWG model, additional statistical measures are employed, namely the determination coefficient (R^2), Root Mean Square Error (RMSE), and Mean Bias Error (MBE), which are calculated using equations (5), (6), and (7) respectively. R^2, is bounded between 0 and 1, and its ideal value is $R^2 = 1$.

$$R = \frac{\sum_i^n (x-\bar{x})(y-\bar{y})}{\sqrt{\sum_i^n (x-\bar{x})^2 \Sigma_i^n (y-\bar{y})^2}} \ , \qquad \text{I =1, …,…, n} \quad (5)$$

$$RMSE = \sqrt{\frac{\sum_i^n (P_i - O_i)^2}{n}} \quad (6)$$

$$MBE = \frac{\sum_i^n (P_i - O_i)}{n} \quad (7)$$

In the calibration and validation process of the model, daily time series of Precipitation, maximum temperature, and minimum temperature are used. These data are obtained from the period RP (1990 to 2020), which serves as the baseline years for the analysis. The data is collected from four weather stations located in the study area.

During the computation of site parameters in LARS-WG, a (*.tst) file is generated. This file includes the results of statistical tests that compare the synthetic weather data with the observed weather data. These tests assess the similarity between the two datasets and provide insights into the model's performance. The statistical tests evaluate the daily values of climate variables by comparing the projected values (P_i) with the observed values (O_i). The tests consider the total number of data points (n) used in the analysis.

The (*.tst) file records the statistical test outcomes, providing valuable information about the agreement between the synthetic and observed weather data. It helps evaluate the accuracy and reliability of the generated climate data concerning the observed climate.

Results

Model Calibration and Validation

A thorough calibration and validation process was conducted to ensure the reliability and credibility of the LARS-WG model in forecasting maximum temperature, minimum temperature, and precipitation for future scenarios. The calibration procedure involved comparing the model results with the seasonal observed data presented in Table 3, while validation was performed by assessing the simulated daily rainfall for each month, as shown in Table 4. The number of tests conducted is denoted by N in both tables, reflecting the sample size used for evaluation.

Journal of Ecohumanism
2024
Volume: 3, No: 8, pp. 2207 – 2234
ISSN: 2752-6798 (Print) | ISSN 2752-6801 (Online)
https://ecohumanism.co.uk/joe/ecohumanism
DOI: https://doi.org/10.62754/joe.v3i8.4898

The findings in Tables 3 and 4 demonstrate that the LARS-WG model exhibits strong capabilities in simulating weather patterns across all monitoring stations, encompassing wet and dry series distributions. Particularly, the model performed exceptionally well during the winter season (DJF), showcasing a perfect fit. In the autumn season (SON), the results indicated a good to perfect fit overall, with the exception of Duhok, which exhibited poor performance in wet SON. During the summer months (JJA), the model displayed good to perfect fit, except for Mandili, Kalar, Qara Tapa, and Erbil, which demonstrated poor performance in dry JJA, as well as Khazir and Chamal, which exhibited poor performance in wet conditions. The evaluation of the spring season (MAM) revealed a very good to perfect fit.

Furthermore, the evaluations presented in Table 4 demonstrate that the LARS-WG model's ability to simulate daily rainfall distributions varied from very good to perfect fit across most months, except for the summer months, where the fit was deemed poor. This can be attributed to the limited rainfall during those months, resulting in challenges in accurately capturing the rainfall patterns through simulation.

The LARS-WG model demonstrated a good overall fit in simulating daily rainfall. However, it is important to acknowledge that achieving high concordance between observed and computed precipitation values is complex due to intermediary processes such as humidity and cloud cover, as highlighted in previous research.

Statistical analyses were conducted to further enhance the confidence in the model's forecasting capabilities by comparing the simulated data with the corresponding observed data. Fig. 2 presents charts illustrating the monthly mean and standard deviation of the generated data, both historical and simulated, for precipitation, minimum, and maximum temperature in the study area. These analyses comprehensively assess the model's performance and its potential for reliable predictions in future scenarios.

Journal of Ecohumanism
2024
Volume: 3, No: 8, pp. 2207 – 2234
ISSN: 2752-6798 (Print) | ISSN 2752-6801 (Online)
https://ecohumanism.co.uk/joe/ecohumanism
DOI: https://doi.org/10.62754/joe.v3i8.4898

Table 3. K–S Test for Distributions of The Seasonal Wet and Dry Series

	Season	Wet/dry	N	K–S	P value	Assessment
Alton Kupri station	DJF	wet	12	0.063	1	Perfect
	DJF	dry	12	0.048	1	Perfect
	MAM	wet	12	0.095	1	Perfect
	MAM	dry	12	0.134	0.978	Very good
	JJA	wet	12	0.174	0.842	Very good
	JJA	dry	12	0.174	0.842	Very good
	SON	wet	12	0.052	1	Perfect
	SON	dry	12	0.072	1	Perfect
Cham Chamal station	DJF	wet	12	0.096	1	Perfect
	DJF	dry	12	0.059	1	Perfect
	MAM	wet	12	0.107	0.999	Very good
	MAM	dry	12	0.095	1	Perfect
	JJA	wet	12	0.647	0	Poor
	JJA	dry	12	0.101	1	Perfect
	SON	wet	12	0.096	1	Perfect
	SON	dry	12	0.077	1	Perfect
Dibiga station	DJF	wet	12	0.073	1	Perfect
	DJF	dry	12	0.046	1	Perfect
	MAM	wet	12	0.111	0.998	Very good
	MAM	dry	12	0.081	1	Perfect
	JJA	wet	12	0.131	0.982	Very good
	JJA	dry	12	0.218	0.589	Good
	SON	wet	12	0.113	0.997	Very good
	SON	dry	12	0.06	1	Perfect
Duhok station	DJF	wet	12	0.068	1	Perfect
	DJF	dry	12	0.056	1	Perfect
	MAM	wet	12	0.066	1	Perfect
	MAM	dry	12	0.113	0.997	Very good
	JJA	wet	12	0.035	1	Perfect
	JJA	dry	12	0.13	0.984	Very good
	SON	wet	12	0.312	0.173	Poor
	SON	dry	12	0.061	1	Perfect
Erbil station	DJF	wet	12	0.079	1	Perfect
	DJF	dry	12	0.072	1	Perfect
	MAM	wet	12	0.084	1	Perfect
	MAM	dry	12	0.086	1	Perfect
	JJA	wet	12	0.086	1	Perfect
	JJA	dry	12	0.312	0.173	Poor
	SON	wet	12	0.057	1	Perfect
	SON	dry	12	0.099	1	Perfect
Kalar station	DJF	wet	12	0.085	1	Perfect
	DJF	dry	12	0.068	1	Perfect
	MAM	wet	12	0.09	1	Perfect
	MAM	dry	12	0.082	1	Perfect
	JJA	wet	12	0.087	1	Perfect
	JJA	dry	12	0.217	0.595	Poor
	SON	wet	12	0.055	1	Perfect
	SON	dry	12	0.087	1	Perfect
Khazir station	DJF	wet	12	0.071	1	Perfect
	DJF	dry	12	0.036	1	Perfect
	MAM	wet	12	0.068	1	Perfect
	MAM	dry	12	0.122	0.992	Very good
	JJA	wet	12	0.582	0	Poor
	JJA	dry	12	0.212	0.625	good
	SON	wet	12	0.055	1	Perfect
	SON	dry	12	0.049	1	Perfect
Kirkuk station	DJF	wet	12	0.063	1	Perfect
	DJF	dry	12	0.082	1	Perfect
	MAM	wet	12	0.064	1	Perfect
	MAM	dry	12	0.086	1	Perfect
	JJA	wet	12	0.174	0.842	Very good
	JJA	dry	12	0.218	0.589	Good
	SON	wet	12	0.071	1	Perfect
	SON	dry	12	0.083	1	Perfect
Makhmur station	DJF	wet	12	0.069	1	Perfect
	DJF	dry	12	0.076	1	Perfect
	MAM	wet	12	0.069	1	Perfect
	MAM	dry	12	0.106	0.999	Very good
	JJA	wet	12	0.174	0.842	Very good
	JJA	dry	12	0.174	0.842	Very good
	SON	wet	12	0.098	1	Perfect
	SON	dry	12	0.049	1	Perfect
Mandili station	DJF	wet	12	0.066	1	Perfect
	DJF	dry	12	0.08	1	Perfect
	MAM	wet	12	0.049	1	Perfect
	MAM	dry	12	0.088	1	Perfect
	JJA	wet	12	0.174	0.842	Very good
	JJA	dry	12	0.305	0.193	Poor
	SON	wet	12	0.069	1	Perfect
	SON	dry	12	0.035	1	Perfect
Qara Tapa station	DJF	wet	12	0.091	1	Perfect
	DJF	dry	12	0.085	1	Perfect
	MAM	wet	12	0.05	1	Perfect
	MAM	dry	12	0.081	1	Perfect
	JJA	wet	12	0.218	0.589	Good
	JJA	dry	12	0.261	0.359	Poor
	SON	wet	12	0.071	1	Perfect
	SON	dry	12	0.056	1	Perfect
Sinjar station	DJF	wet	12	0.079	1	Perfect
	DJF	dry	12	0.04	1	Perfect
	MAM	wet	12	0.094	1	Perfect
	MAM	dry	12	0.161	0.901	Very good
	JJA	wet	12	0.048	1	Perfect
	JJA	dry	12	0.157	0.916	Very good
	SON	wet	12	0.212	0.625	Good
	SON	dry	12	0.042	1	Perfect
West Tigris River station	DJF	wet	12	0.06	1	Perfect
	DJF	dry	12	0.067	1	Perfect
	MAM	wet	12	0.102	0.999	Very good
	MAM	dry	12	0.113	0.997	Very good
	JJA	wet	12	0.174	0.842	Very good
	JJA	dry	12	0.13	0.984	Very good
	SON	wet	12	0.071	1	Perfect
	SON	dry	12	0.052	1	Perfect

Journal of Ecohumanism
2024
Volume: 3, No: 8, pp. 2207 – 2234
ISSN: 2752-6798 (Print) | ISSN 2752-6801 (Online)
https://ecohumanism.co.uk/joe/ecohumanism
DOI: https://doi.org/10.62754/joe.v3i8.4898

Table 4: K–S-test for distributions of daily rainfall

	Month	N	K–S	P value	Assessment
Alton Kupri station	J	12	0.042	1	Perfect
	F	12	0.08	1	Perfect
	M	12	0.121	0.993	Very good
	A	12	0.078	1	Perfect
	M	12	0.042	1	Perfect
	J	12	0.348	0.096	Poor
	J		No precipitation		
	A	12	1	0	Poor
	S	12	0.565	0.001	Poor
	O	12	0.066	1	Perfect
	N	12	0.027	1	Perfect
	D	12	0.074	1	Perfect
Cham Chamal station	J	12	0.137	0.972	Very good
	F	12	0.047	1	Perfect
	M	12	0.051	1	Perfect
	A	12	0.093	1	Perfect
	M	12	0.052	1	Perfect
	J	12	0.079	1	Perfect
	J	12	0.435	0.017	Poor
	A	12	0.609	0	Poor
	S	12	0.355	0.084	Poor
	O	12	0.083	1	Perfect
	N	12	0.049	1	Perfect
	D	12	0.044	1	Perfect
Dibiga station	J	12	0.08	1	Perfect
	F	12	0.085	1	Perfect
	M	12	0.081	1	Perfect
	A	12	0.063	1	Perfect
	M	12	0.045	1	Perfect
	J	12	0.348	0.096	Poor
	J		No precipitation		
	A	12	1	0	Poor
	S	12	0.566	0.001	Poor
	O	12	0.038	1	Perfect
	N	12	0.063	1	Perfect
	D	12	0.082	1	Perfect

	Month	N	K–S	P value	Assessment
Duhok station	J	12	0.138	0.971	
	F	12	0.011	1	Perfect
	M	12	0.088	1	Perfect
	A	12	0.059	1	Perfect
	M	12	0.058	1	Perfect
	J	12	0.086	1	Perfect
	J	12	1	0	Poor
	A	12	0.392	0.042	Poor
	S	12	0.147	0.949	Very good
	O	12	0.056	1	Perfect
	N	12	0.072	1	Perfect
	D	12	0.048	1	Perfect
Erbil station	J	12	0.052	1	Perfect
	F	12	0.058	1	Perfect
	M	12	0.07	1	Perfect
	A	12	0.074	1	Perfect
	M	12	0.063	1	Perfect
	J	12	0.042	1	Perfect
	J	12	1	0	
	A	12	0.391	0.043	Poor
	S	12	0.293	0.231	Poor
	O	12	0.072	1	Perfect
	N	12	0.07	1	Perfect
	D	12	0.037	1	Perfect
Kalar station	J	12	0.065	1	Perfect
	F	12	0.044	1	Perfect
	M	12	0.088	1	Perfect
	A	12	0.059	1	Perfect
	M	12	0.033	1	Perfect
	J	12	0.435	0.017	Poor
	J	12	0.652	0	Poor
	A	12	1	0	Poor
	S	12	0.566	0.001	Poor
	O	12	0.063	1	Perfect
	N	12	0.101	1	Perfect
	D	12	0.035	1	Perfect

	Month	N	K–S	P value	Assessment
Khazir station	J	12	0.071	1	Perfect
	F	12	0.015	1	Perfect
	M	12	0.056	1	Perfect
	A	12	0.052	1	Perfect
	M	12	0.064	1	Perfect
	J	12	0.104	0.999	Very good
	J	12	1	0	Poor
	A	12	0.391	0.043	Poor
	S	12	0.429	0.02	Poor
	O	12	0.077	1	Perfect
	N	12	0.069	1	Perfect
	D	12	0.037	1	Perfect
Kirkuk station	J	12	0.038	1	Perfect
	F	12	0.059	1	Perfect
	M	12	0.11	0.998	
	A	12	0.104	0.999	
	M	12	0.039	1	Perfect
	J	12	0.692	0	Poor
	J		No precipitation		
	A	12	1	0	Poor
	S	12	0.435	0.017	Poor
	O	12	0.058	1	Perfect
	N	12	0.026	1	Perfect
	D	12	0.081	1	Perfect
Makhmur station	J	12	0.049	1	Perfect
	F	12	0.041	1	Perfect
	M	12	0.111	0.998	
	A	12	0.038	1	Perfect
	M	12	0.053	1	Perfect
	J	12	0.522	0.002	Poor
	J		No precipitation		
	A	12	1	0	Poor
	S	12	0.261	0.359	Poor
	O	12	0.05	1	Perfect
	N	12	0.04	1	Perfect
	D	12	0.108	0.999	Very good

	Month	N	K–S	P value	Assessment
Mandili station	J	12	0.041	1	Perfect
	F	12	0.038	1	Perfect
	M	12	0.099	1	Perfect
	A	12	0.079	1	Perfect
	M	12	0.085	1	Perfect
	J	12	0.522	0.002	Poor
	J	12	1	0	Poor
	A		No precipitation		
	S	12	0.348	0.096	Poor
	O	12	0.043	1	Perfect
	N	12	0.035	1	Perfect
	D	12	0.062	1	Perfect
Qara Tapa station	J	12	0.065	1	Perfect
	F	12	0.045	1	Perfect
	M	12	0.078	1	Perfect
	A	12	0.098	1	Perfect
	M	12	0.048	1	Perfect
	J	12	0.522	0.002	Poor
	J	12	1	0	Poor
	A		No precipitation		
	S	12	0.43	0.019	Poor
	O	12	0.055	1	Perfect
	N	12	0.057	1	Perfect
	D	12	0.084	1	Perfect
Sinjar station	J	12	0.084	1	Perfect
	F	12	0.038	1	Perfect
	M	12	0.045	1	Perfect
	A	12	0.062	1	Perfect
	M	12	0.03	1	Perfect
	J	12	0.158	0.913	Very good
	J	12	1	0	Poor
	A	12	0.479	0.006	Poor
	S	12	0.05	1	Perfect
	O	12	0.064	1	Perfect
	N	12	0.067	1	Perfect
	D	12	0.063	1	Perfect

	Month	N	K–S	P value	Assessment
West Tigris River station	J	12	0.042	1	Perfect
	F	12	0.071	1	Perfect
	M	12	0.074	1	Perfect
	A	12	0.044	1	Perfect
	M	12	0.046	1	Perfect
	J	12	0.609	0	Poor
	J	12	1	0	Poor
	A	12	0.609	0	Poor
	S	12	0.261	0.359	Poor
	O	12	0.032	1	Perfect
	N	12	0.097	1	Perfect
	D	12	0.032	1	Perfect

Journal of Ecohumanism
2024
Volume: 3, No: 8, pp. 2207 – 2234
ISSN: 2752-6798 (Print) | ISSN 2752-6801 (Online)
https://ecohumanism.co.uk/joe/ecohumanism
DOI: https://doi.org/10.62754/joe.v3i8.4898

The assessment of the LARS-WG model's performance in generating average monthly temperatures and precipitation at the selected stations is presented in Table 5 and Figure 3. These evaluations include the root-mean-square error (RMSE), mean bias error (MBE), and coefficient of determination (R^2) between the observed and simulated data.

Figure 3 provides a visual representation of the R^2 values, which indicate the strength of the linear relationship between the observed and simulated data. Across all three climate variables (average monthly maximum temperature, minimum temperature, and precipitation), the R^2 values range from 0.942 to 0.999. These high R^2 values suggest a robust linear association between the observed and simulated data, reinforcing the model's ability to capture the variations in temperature and precipitation accurately.

The RMSE values, displayed in Table 5, reflect the average magnitude of the differences between the observed and simulated values. The RMSE values range from 0.118 to 8.28, indicating the level of variation or dispersion in the model's performance for different climate variables.

Meanwhile, the MBE values, also presented in Table 5, represent the mean bias or the average deviation between the observed and simulated data. The MBE values range from -2.127 to 1.92, providing insights into the systematic overestimation or underestimation of the model predictions.

Overall, the LARS-WG model reasonably generates average monthly temperatures and precipitation at the selected stations. The strong linear association between the observed and simulated data, as indicated by high R^2 values, validates the model's ability to reproduce the climate variables accurately. Although some variability and biases are present, as reflected by the RMSE and MBE values, the model's performance overall allows for its practical application in future weather forecasting endeavours.

Table 5. Results of the Model of Calibration and Validation for T_{max}, T_{min} and Precipitation

Station	Climate Variable	R^2	RMSE	MBE	Station	Climate Variable	R^2	RMSE	MBE
Sinjar	Tmax	0.9998	0.176	0.042	**Alton Kupri**	Tmax	0.9998	0.192	0.006
	Tmin	O.9997	0.150	-0.068		Tmin	0.9995	0.178	-0.049
	Precipitation	0.995	3.410	-2.128		Precipitation	0.9788	4.296	-2.117
Duhok	Tmax	0.9997	0.228	-0.077	**Kirkuk**	Tmax	0.9997	0.254	-0.029
	Tmin	0.9995	0.193	-0.033		Tmin	0.9996	0.207	-0.005
	Precipitation	0.9812	7.840	0.981		Precipitation	0.9421	6.112	-1.252
West Tigris River	Tmax	0.9999	0.153	0.052	**Cham Chamal**	Tmax	0.9999	0.173	-0.003
	Tmin	0.9997	0.156	-0.070		Tmin	0.9996	0.166	-0.027
	Precipitation	0.96	2.576	-0.763		Precipitation	0.9766	8.280	0.764
Khazir	Tmax	0.9997	0.304	-0.082	**Kalar**	Tmax	0.9996	0.219	0.012
	Tmin	0.9999	0.126	-0.007		Tmin	0.9994	0.214	0.037
	Precipitation	0.9882	4.905	-0.434		Precipitation	0.962	3.908	-0.657
Erbil	Tmax	0.9996	0.260	-0.039	**Qara Tapa**	Tmax	0.9998	0.190	-0.001
	Tmin	0.9999	0.118	0.023		Tmin	0.9997	0.162	-0.018
	Precipitation	0.9801	7.170	1.920		Precipitation	0.9863	2.208	-1.090
Dibiga	Tmax	0.9998	0.182	-0.062	**Mandili**	Tmax	0.9998	0.216	-0.013
	Tmin	0.9996	0.149	-0.015		Tmin	0.9998	0.149	-0.077
	Precipitation	0.9775	3.810	0.570		Precipitation	0.9884	2.170	-1.149
Makhmur	Tmax	0.9998	0.153	0.050					
	Tmin	0.9924	0.837	-0.287					
	Precipitation	0.9632	3.010	0.022					

Journal of Ecohumanism
2024
Volume: 3, No: 8, pp. 2207 – 2234
ISSN: 2752-6798 (Print) | ISSN 2752-6801 (Online)
https://ecohumanism.co.uk/joe/ecohumanism
DOI: https://doi.org/10.62754/joe.v3i8.4898

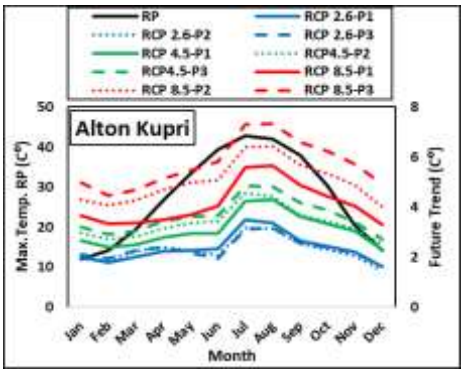

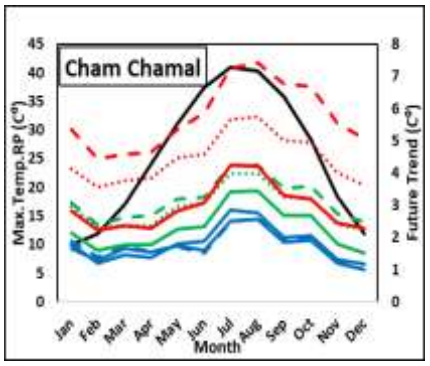

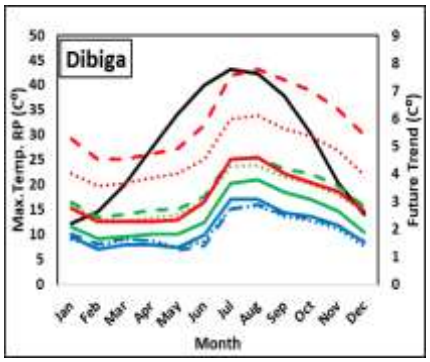

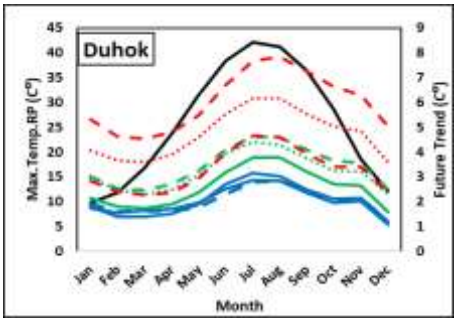

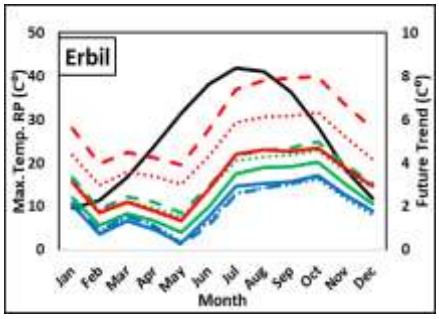

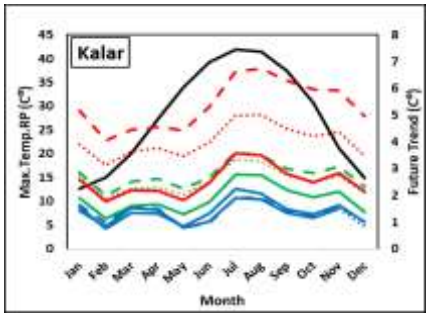

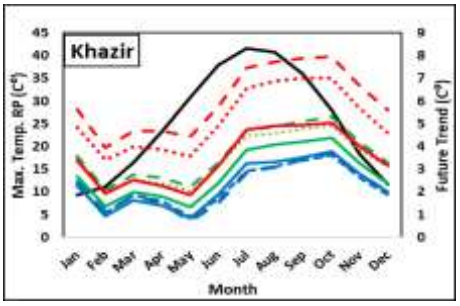

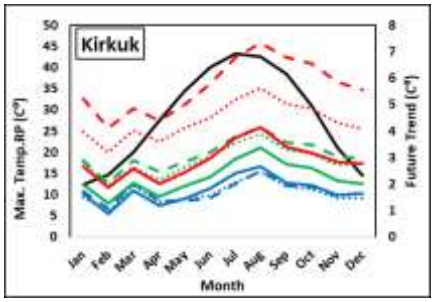

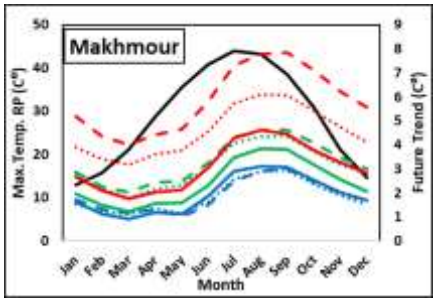

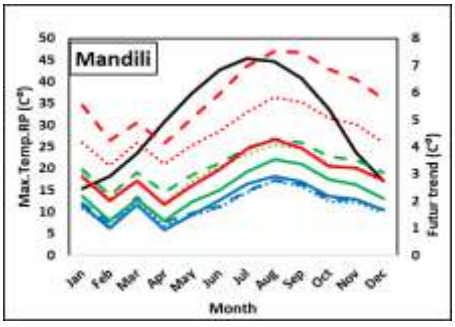

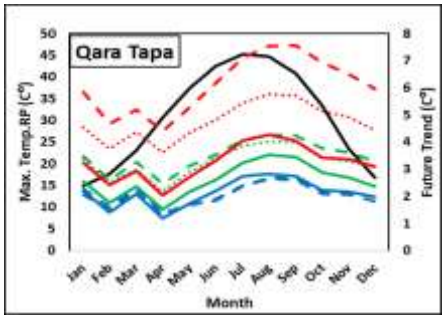

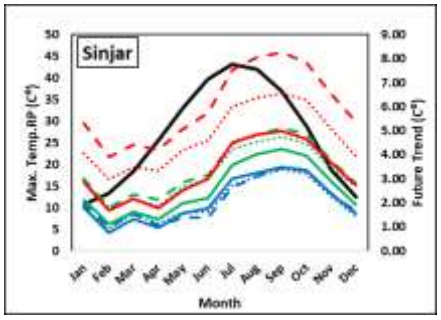

Journal of Ecohumanism
2024
Volume: 3, No: 8, pp. 2207 – 2234
ISSN: 2752-6798 (Print) | ISSN 2752-6801 (Online)
https://ecohumanism.co.uk/joe/ecohumanism
DOI: https://doi.org/10.62754/joe.v3i8.4898

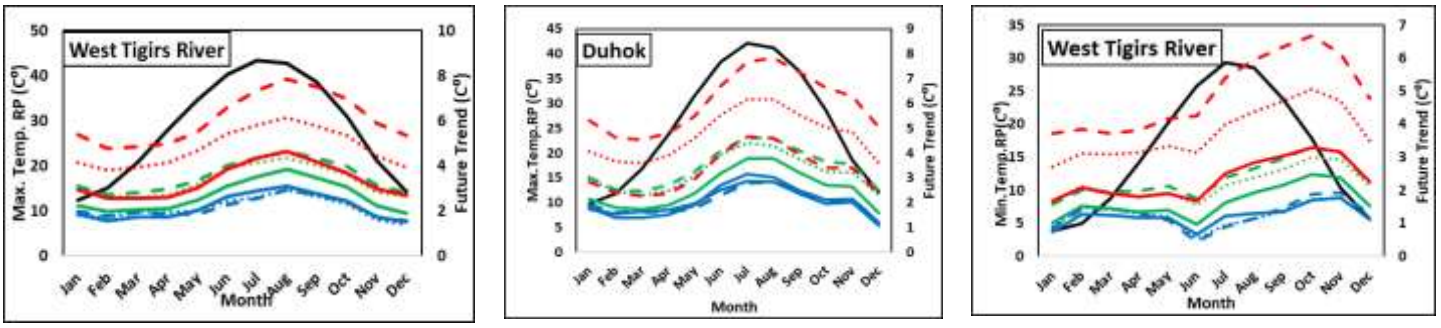

Fig. 4. Future Trend in Maximum Temperature. (The Primary Y-Axis (Left)Represents Maximum Temperature In RP, Secondary Y-Axis (Right) Represents the Future Trend of Maximum Temperature)

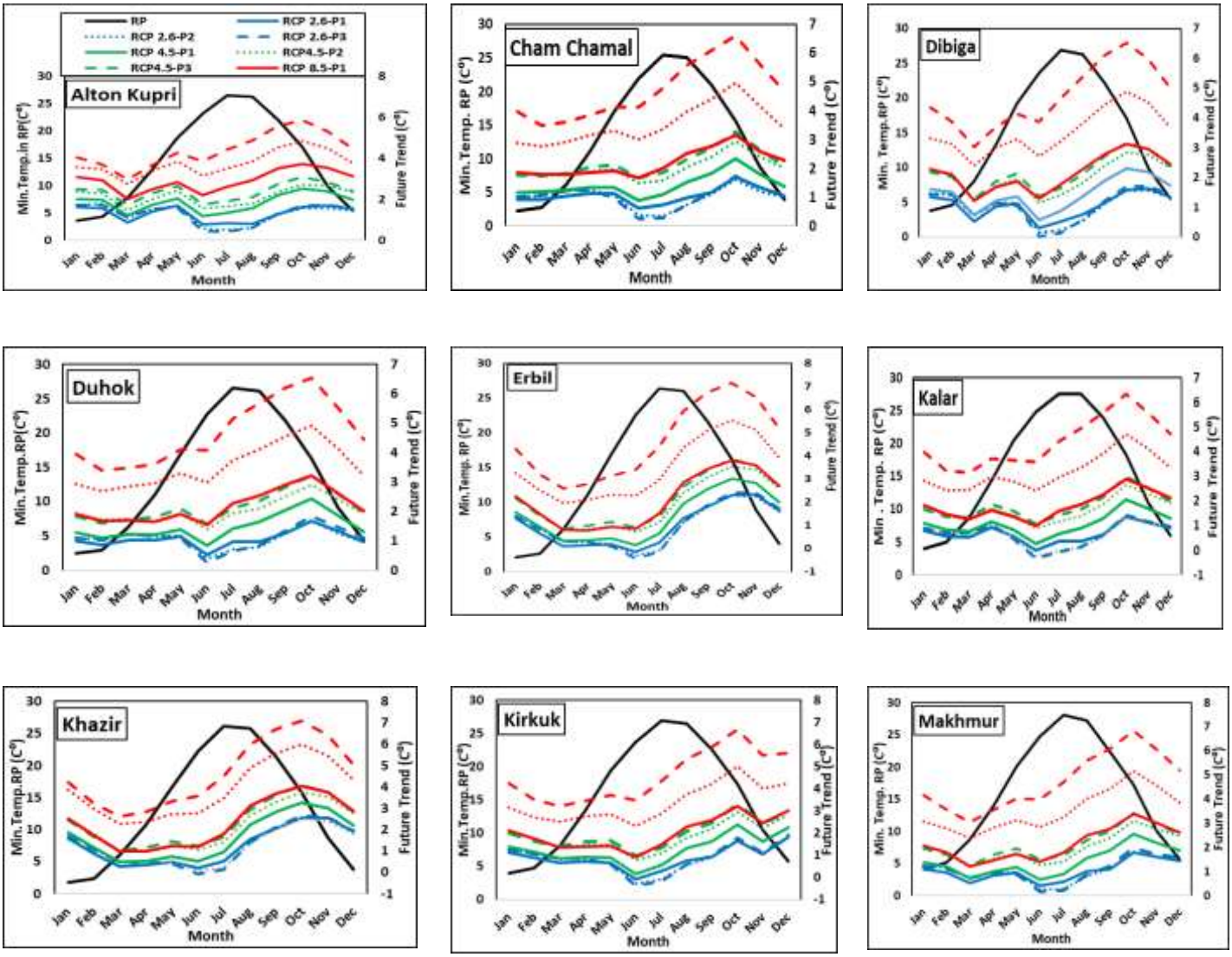

Journal of Ecohumanism
2024
Volume: 3, No: 8, pp. 2207 – 2234
ISSN: 2752-6798 (Print) | ISSN 2752-6801 (Online)
https://ecohumanism.co.uk/joe/ecohumanism
DOI: https://doi.org/10.62754/joe.v3i8.4898

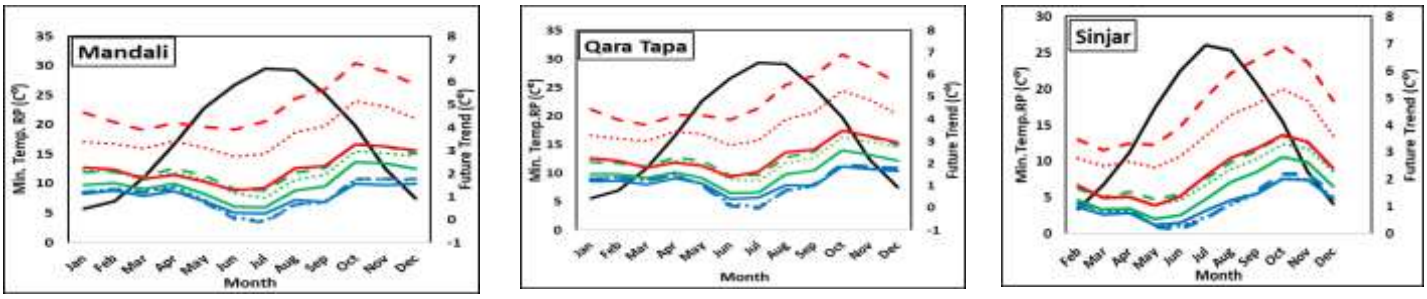

Fig .5: Future trend in minimum temperature. (The primary y-axis (left)represents maximum temperature in RP, secondary y-axis (right) represents the future trend of maximum temperature)

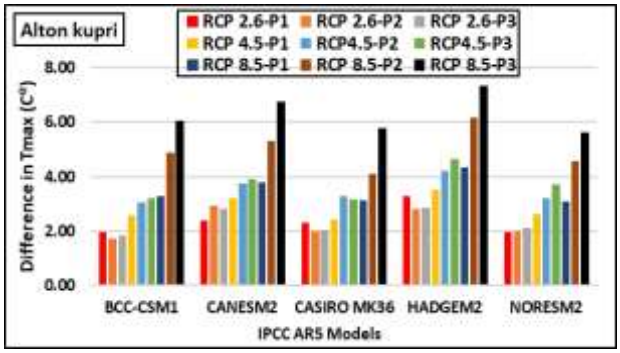

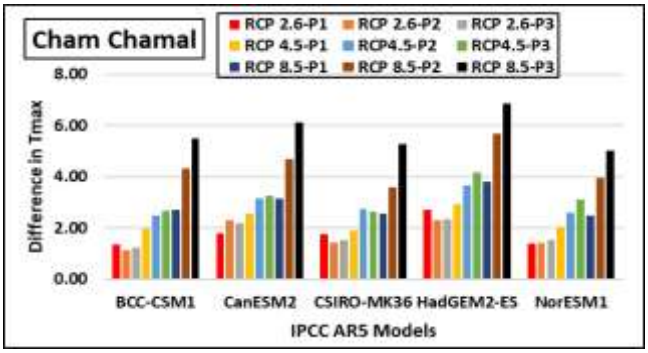

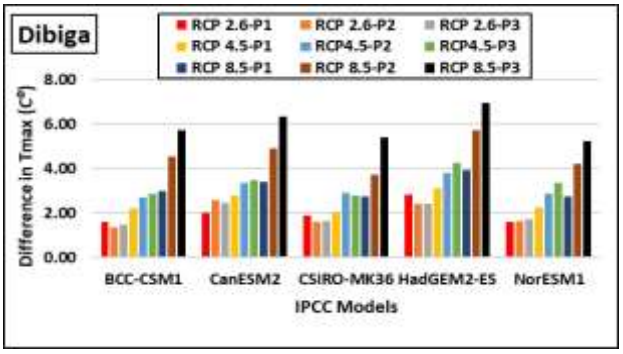

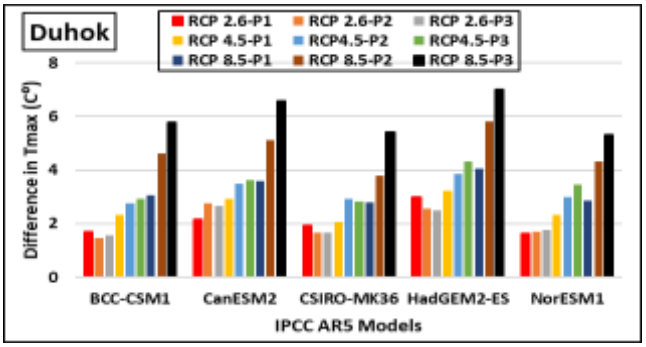

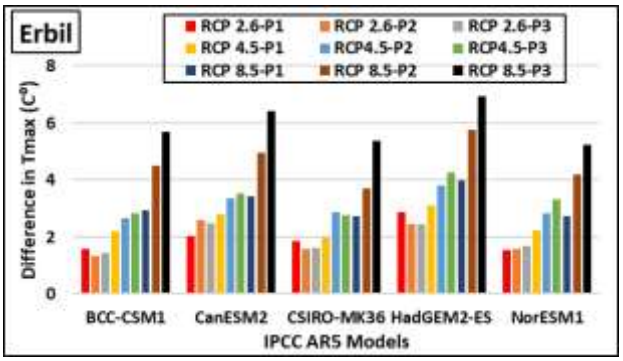

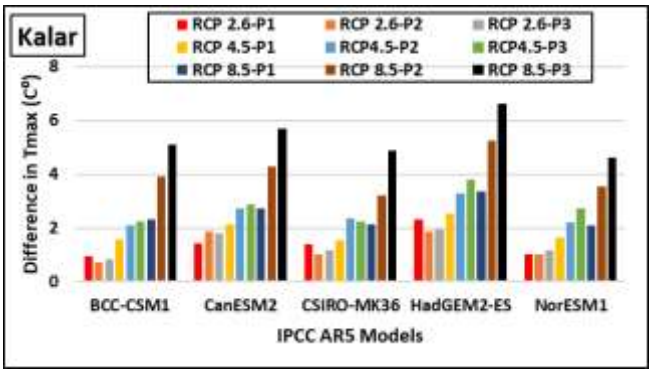

Journal of Ecohumanism
2024
Volume: 3, No: 8, pp. 2207 – 2234
ISSN: 2752-6798 (Print) | ISSN 2752-6801 (Online)
https://ecohumanism.co.uk/joe/ecohumanism
DOI: https://doi.org/10.62754/joe.v3i8.4898

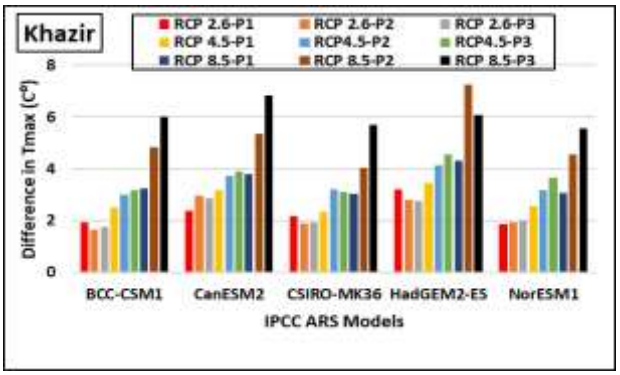

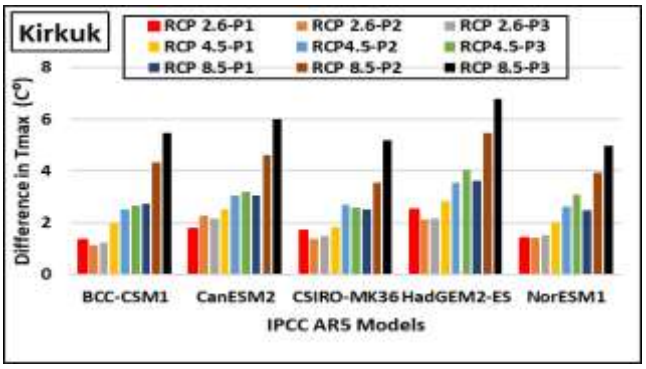

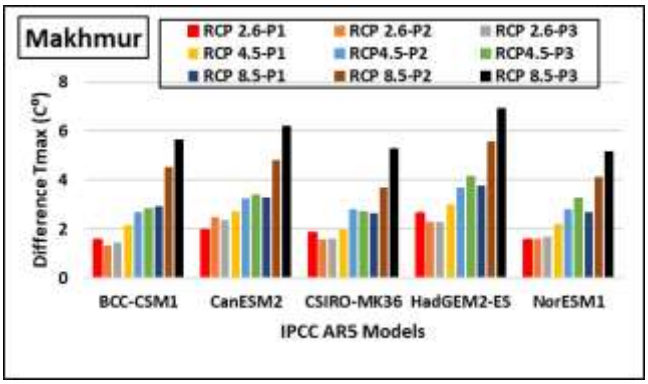

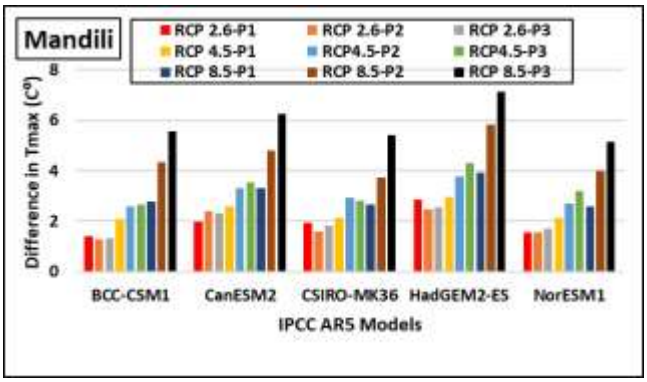

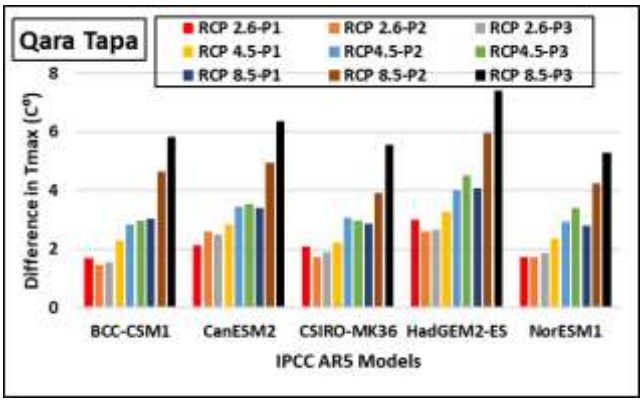

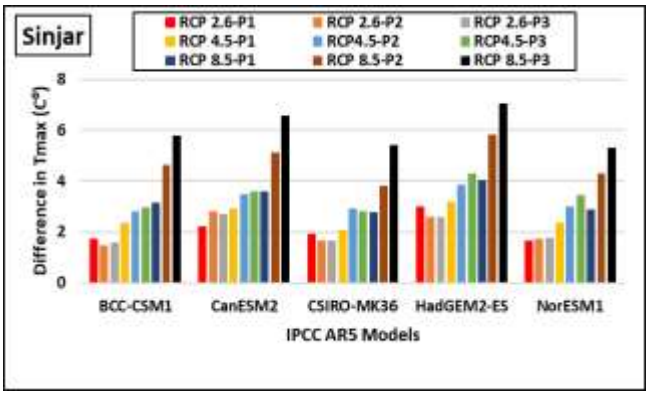

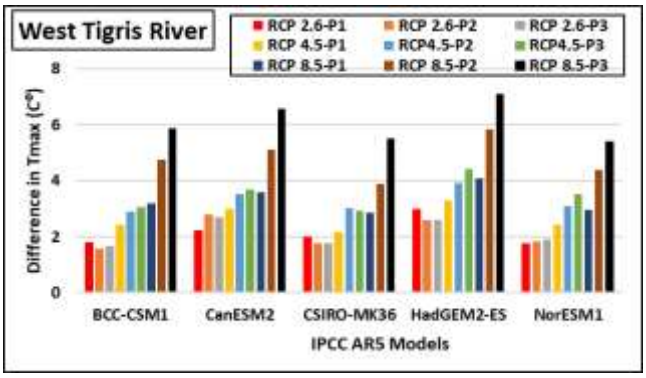

Journal of Ecohumanism
2024
Volume: 3, No: 8, pp. 2207 – 2234
ISSN: 2752-6798 (Print) | ISSN 2752-6801 (Online)
https://ecohumanism.co.uk/joe/ecohumanism
DOI: https://doi.org/10.62754/joe.v3i8.4898

Fig.6. Annual Max Temperatures Differences Between Three Periods P1,P2 And P3 And Observed Period (1990–2020)

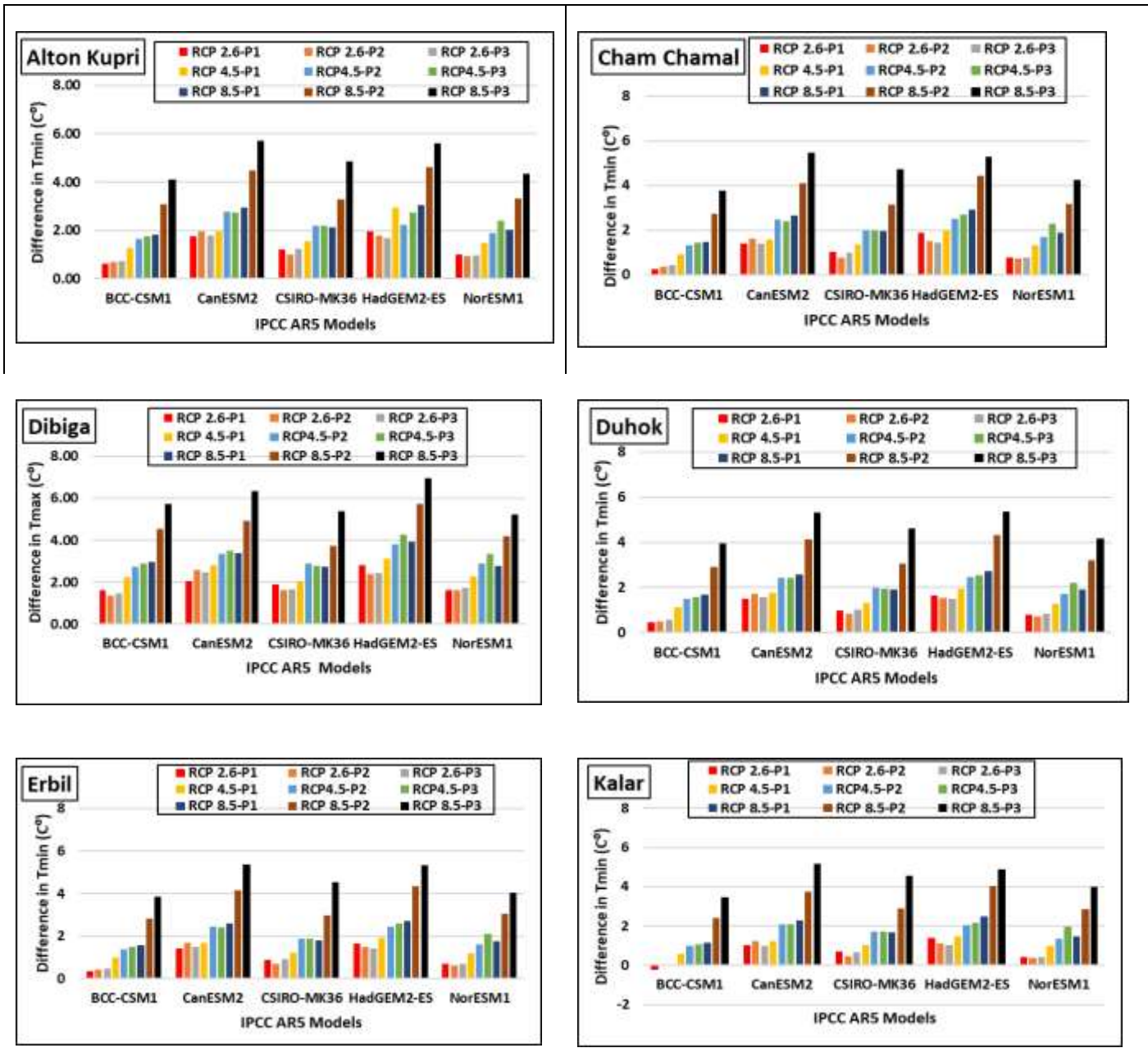

Journal of Ecohumanism
2024
Volume: 3, No: 8, pp. 2207 – 2234
ISSN: 2752-6798 (Print) | ISSN 2752-6801 (Online)
https://ecohumanism.co.uk/joe/ecohumanism
DOI: https://doi.org/10.62754/joe.v3i8.4898

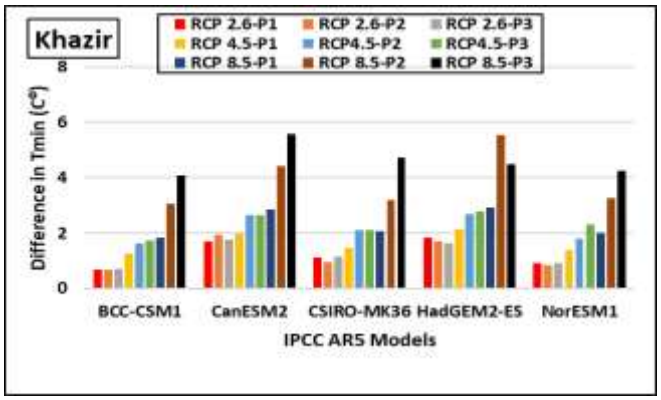

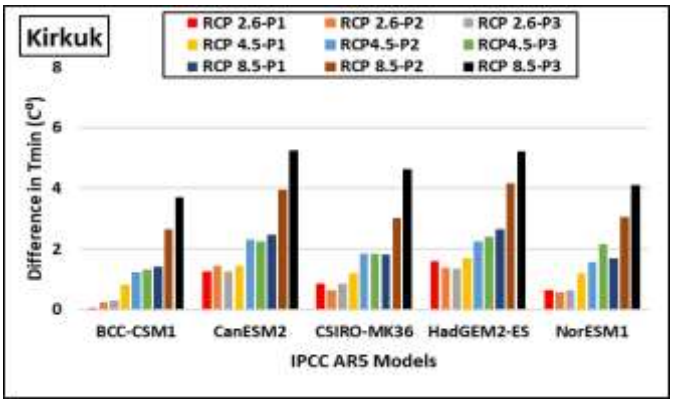

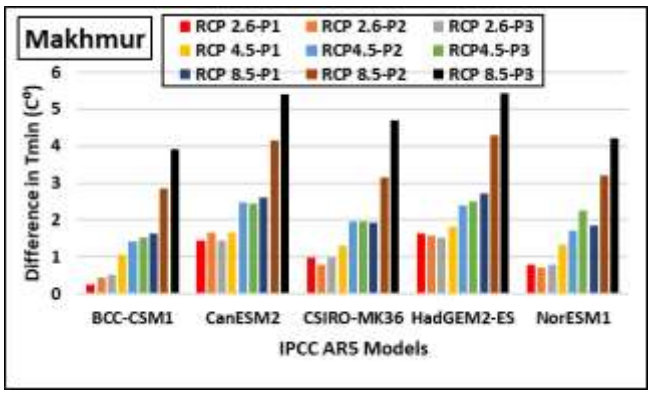

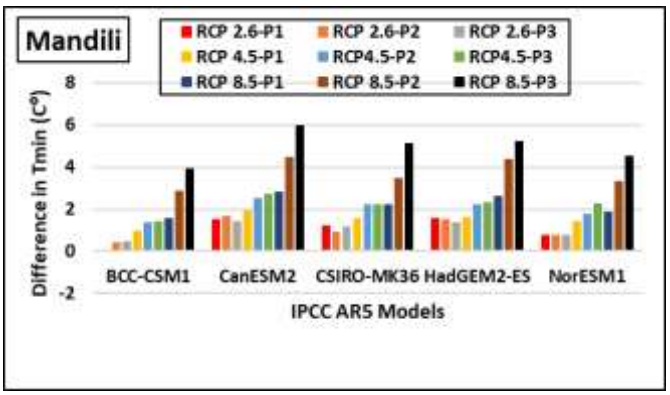

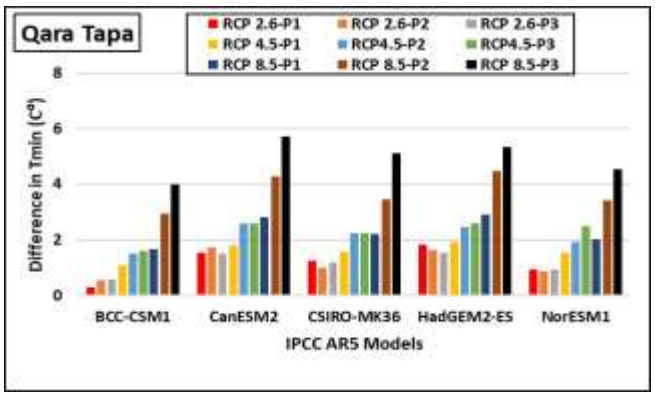

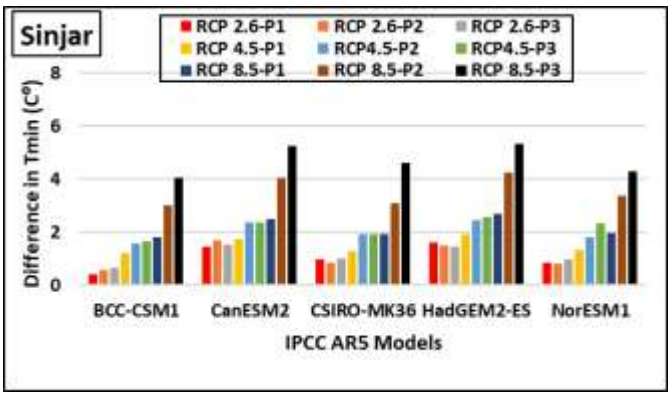

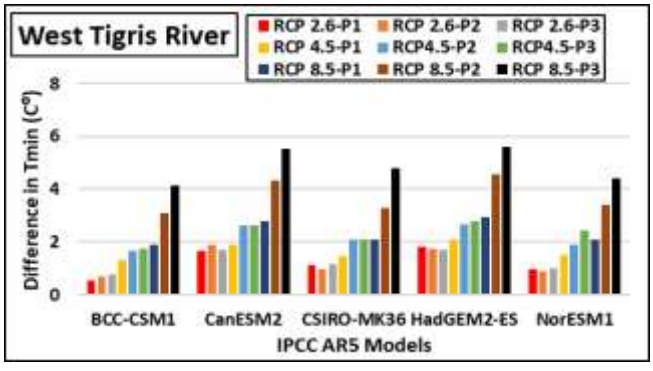

Journal of Ecohumanism
2024
Volume: 3, No: 8, pp. 2207 – 2234
ISSN: 2752-6798 (Print) | ISSN 2752-6801 (Online)
https://ecohumanism.co.uk/joe/ecohumanism
DOI: https://doi.org/10.62754/joe.v3i8.4898

Fig. 7 Annual Tmin Differences Between Three Periods (2040–2060, 2060–2080, 2080–2100) And Observed Period (1990–2020)

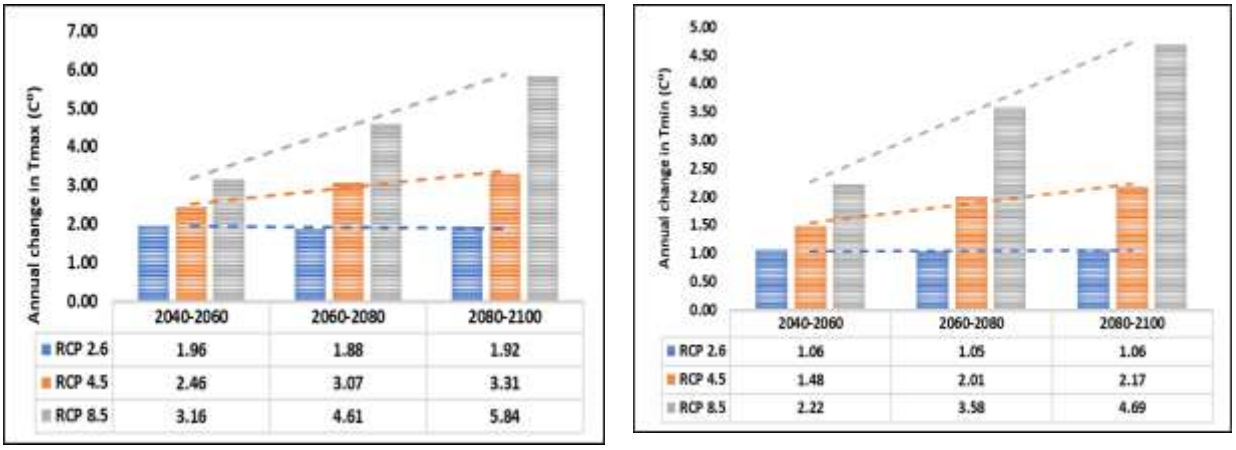

Fig. 8 Changes In Predicted Annual Maximum And Minimum Temperatures n Tthe Future or Average of the 13 Selected Stations(Low Folded Zone)

Projection of Future Temperatures

After calibrating and validating the LARS-WG model, a weather generator model was constructed for each chosen station in Iraq's research area. Subsequently, this model was utilized to forecast forthcoming daily precipitation, maximum temperatures, and minimum temperatures for the time spanning from 2040 to 2100. The future period was divided into three distinct intervals: P1 (2040-2060), P2 (2060-2080), and P3 (2080-2100).

Five distinct Global Circulation Models (GCMs), specifically BCC-CSM1, CanESM2, CSIRO-MK36, HadGEM2-ES, and NorESM1, were employed alongside three different scenarios: RCP2.6, RCP4.5, and RCP8.5.

The outcomes pertaining to the future temperatures are presented in Figures 4, 5,6 and 7. Figure 4,5 portrays the average monthly temperatures observed during the reference period (1990-2020) as well as the average values projected by the five GCMs for the three future periods (P1, P2, and P3) under the three scenarios (RCP2.6, RCP4.5, and RCP8.5). The charts exhibit a consistent escalation in maximum (T_{max}) and minimum (T_{min}) temperatures over time for all stations and under each scenario. The lowest values of Tmax and Tmin were documented during the reference period (RP), while the highest values were observed during the distant future period (P3). It is noteworthy that January exhibits the lowest average temperatures, whereas July and August endure the highest average temperatures across all thirteen stations. The Qara Tapa station is projected to encounter the highest maximum temperatures during the far future period (P3) under the RCP8.5 scenario, with a peak value of 52.34 °C in July.

The annual temperature disparities between the three future periods the selected five GCMs anticipated and the observed reference period. The charts show that the average annual maximum temperatures will rise during the twenty-first century for all 13 stations; Alton Kupri station, Cham chamal, Dibiga, Duhok, Erbil,kalar, Kirkuk, Khazir, Makhmur, Mandili, Qara Tapa, Sinjar, and West Tigirs River stations, the increase will be between (1.7-1.8),(1.91-1.99), (2.03-2.1) , (1.91-1.98) , (1.3-1.4) (1.66-1.75), (1.91-1.99) , (1.85-1.92) , (1.85-1.94) , (2.02-2.12) , (1.3-1.4) °C under **RCP2.6**, (3.08-3.64), (2.28-3.17), (2.48-3.35) , 2.57-3.43) , (2.47-3.34), (1.88-2.77), (2.23-3.11), (2.8-3.67), (2.23-3.11), (2.42-3.288) , (2.38-3.30) , (2.59-3.47) , (2.58-2.43) °C and (2.66-3.51) °C under **RCP4.5**. (4.12-5.71), (2.9-5.74), (3.15-5.93), (3.26-6.02), (3.15-5.92), (2.52-5.37), (2.88-5.68) , (3.49-6.03), (3.08-5.86), (3.05-5.9), (3.23-6.09), (3.28-6.03) and (3.33-6.08) under **RCP 8.5 .**

Journal of Ecohumanism
2024
Volume: 3, No: 8, pp. 2207 – 2234
ISSN: 2752-6798 (Print) | ISSN 2752-6801 (Online)
https://ecohumanism.co.uk/joe/ecohumanism
DOI: https://doi.org/10.62754/joe.v3i8.4898

In Figure 6,7, the least difference in maximum temperature predictions was observed for the BCC-CSM1 model under the RCP2.6 scenario and the NorESM1-M model under the RCP4.5 and RCP8.5 scenarios. On the other hand, the HadGEM2-ES model exhibited the highest temperature difference for each scenario (RCP2.6, RCP4.5, and RCP8.5). Specifically, at the Qara Tapa station, the highest difference in maximum temperature, reaching approximately 7.41 °C, was observed under the RCP8.5 scenario for the HadGEM2-ES model.

In Figure 8, the average annual increases in Low Folded Zone, minimum and maximum temperatures across all 13 stations are displayed. The results for the RCP8.5 scenario showed the largest difference in temperature range, with values ranging from 3.16 to 5.84 °C for maximum temperature (Tmax) and from 2.22 to 4.69 °C for minimum temperature (Tmin). In the **RCP4.5** scenario, the temperature differences ranged from 2.46 to 3.31 °C for Tmax and from 1.48 to 2.17 °C for Tmin. For the **RCP2.6** scenario, the smallest temperature differences were observed, with values ranging from 1.88 to 1.96 °C for Tmax and from 1.00 to 1.06 °C for Tmin.

Generally, the average predicted temperature increase during the twenty-first century for all 13 selected stations falls between 0.94 and 4.98 °C, as illustrated in Figure 7.

These findings align with previous studies conducted by Salman et al. [36], Pirttioja et al. [37], and Hassan and Hashim [38], providing further support for the robustness of the results.

Future Precipitation Projection

The study area's precipitation patterns analysis reveals interesting variations over time and across different locations. We can clearly see changes in the amount of rainfall, its intensity, the direction it comes from, and even when it occurs throughout the year. One striking observation is the lack of consistent rainfall during the summer months, making it difficult to establish a predictable trend for precipitation in the study area. In fact, it seems like rainfall tends to be quite unpredictable, and there is no significant rain during June, July, August, and September across all the monitoring stations.

Figure 9 To give you an idea of the average annual precipitation during the reference period (1990-2020), Alton Kupri received about 347.73 mm of rain per year, while Cham Chamal had 724.18 mm, and Dibiga had 347.73 mm. Duhok experienced an average of 689.07 mm, Erbil received 594.81 mm, and Kalar had 248.85 mm. Khazir received 594.81 mm, Kirkuk had 347.48 mm, Makhmur had 214.79 mm, Mandili had 210.82 mm, and Qara Tapa had 210.82 mm. Sinjar received 434.43 mm, and the West Tigris River area had 180 mm of annual rainfall.

Looking into the future period from 2040 to 2100 in figure 9, things get even more interesting. The projections show that precipitation patterns will vary depending on different emission scenarios like RCP 2.6, RCP 4.5, and RCP 8.5, as well as specific months. Generally, we can expect a decrease in rainfall in low folded zone during January in RCP 4.5, February ,Mars and April in RCP 4.5 and RCP 8.5, December was decreased in all scenarios

. However, the other months are predicted to experience an increase in rainfall. It's fascinating how these changes differ across the various stations and scenarios.

Figure 10 visualizes the annual difference in precipitation using five different models: (BCC-CSM1,CanESM2,CSIRO-MK36,HadGEM2-ES and NorESM1). By comparing three different periods (P1, P2, and P3), we can clearly see how CanESM2 stands out by predicting the highest increase in precipitation across all scenarios. In fact, the Cham Chamal station, under the RCP 8.5 scenario from 2080 to 2100, shows the most significant increase in rainfall using the CanESM2 model.

Figure 11 show the percentage of increase varies depending on the future period and emission scenario (RCP 2.6, RCP 4.5, or RCP 8.5). For RCP 2.6, we can expect an increase ranging from 7.07% to 10.75%. As for RCP 4.5, the increase is much smaller, ranging from 0% to 2.2%. Finally, under RCP 8.5, the

Journal of Ecohumanism
2024
Volume: 3, No: 8, pp. 2207 – 2234
ISSN: 2752-6798 (Print) | ISSN 2752-6801 (Online)
https://ecohumanism.co.uk/joe/ecohumanism
DOI: https://doi.org/10.62754/joe.v3i8.4898

projected increase falls between 3.7% and 6.8%. These findings are consistent with previous research conducted [38] .

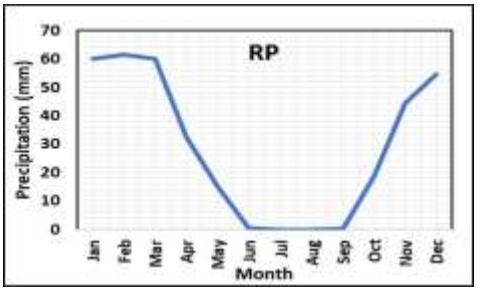
RP
Precipitation (mm)
Month
Jan Feb Mar Apr May Jun Jul Aug Sep Oct Nov Dec

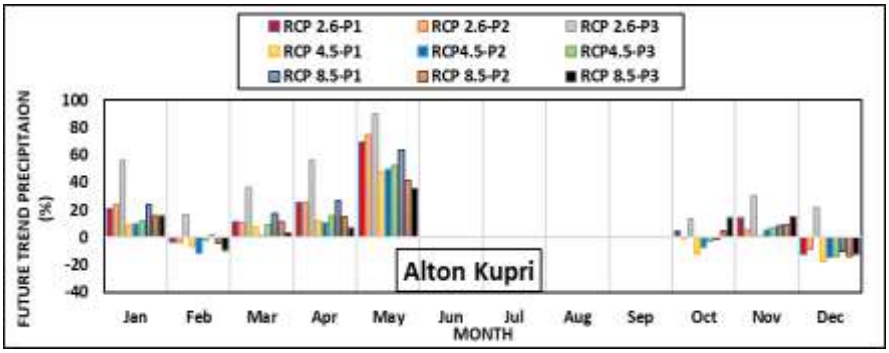
RCP 2.6-P1
RCP 2.6-P2
RCP 2.6-P3
RCP 4.5-P1
RCP4.5-P2
RCP4.5-P3
RCP 8.5-P1
RCP 8.5-P2
RCP 8.5-P3
FUTURE TREND PRECIPITAION (%)
Alton Kupri
MONTH
Jan Feb Mar Apr May Jun Jul Aug Sep Oct Nov Dec

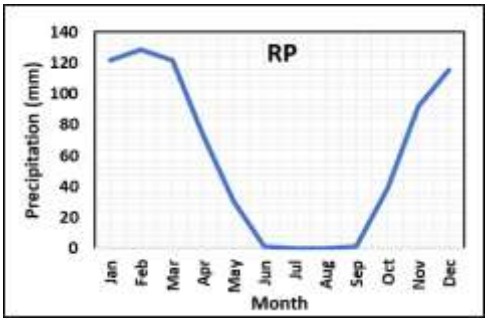
RP
Precipitation (mm)
Month
Jan Feb Mar Apr May Jun Jul Aug Sep Oct Nov Dec

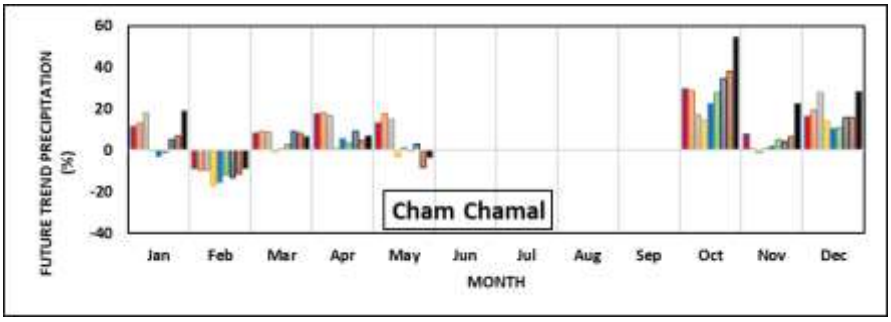
FUTURE TREND PRECIPITATION (%)
Cham Chamal
MONTH
Jan Feb Mar Apr May Jun Jul Aug Sep Oct Nov Dec

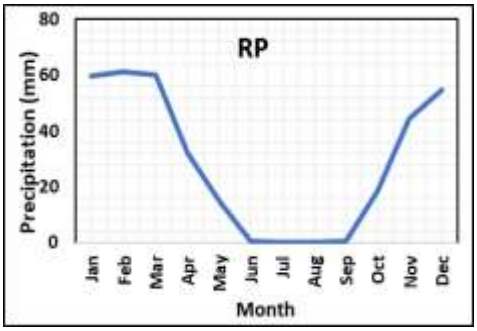
RP
Precipitation (mm)
Month
Jan Feb Mar Apr May Jun Jul Aug Sep Oct Nov Dec

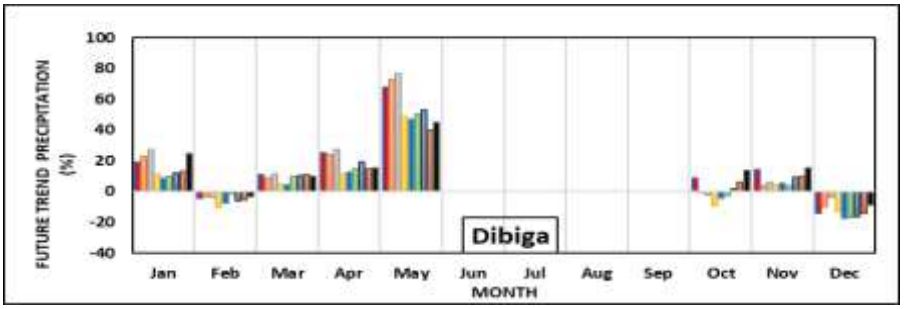
FUTURE TREND PRECIPITATION (%)
Dibiga
MONTH
Jan Feb Mar Apr May Jun Jul Aug Sep Oct Nov Dec

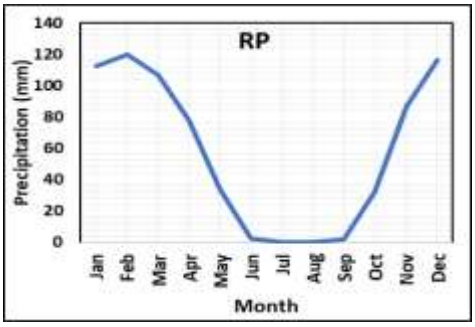
RP
Precipitation (mm)
Month
Jan Feb Mar Apr May Jun Jul Aug Sep Oct Nov Dec

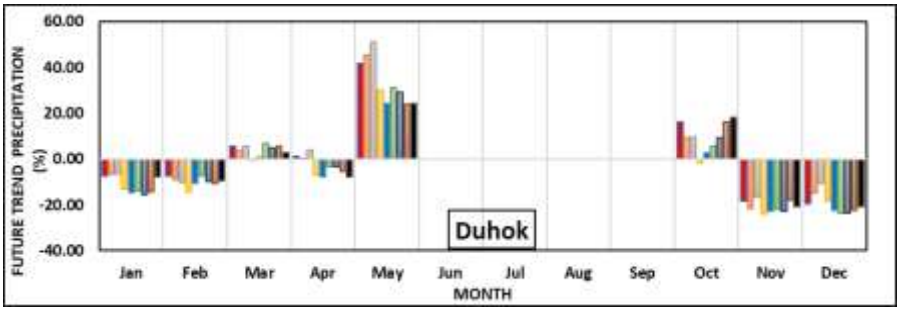
FUTURE TREND PRECIPITATION (%)
Duhok
MONTH
Jan Feb Mar Apr May Jun Jul Aug Sep Oct Nov Dec

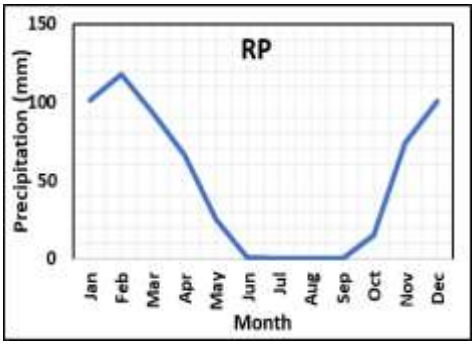
RP
Precipitation (mm)
Month
Jan Feb Mar Apr May Jun Jul Aug Sep Oct Nov Dec

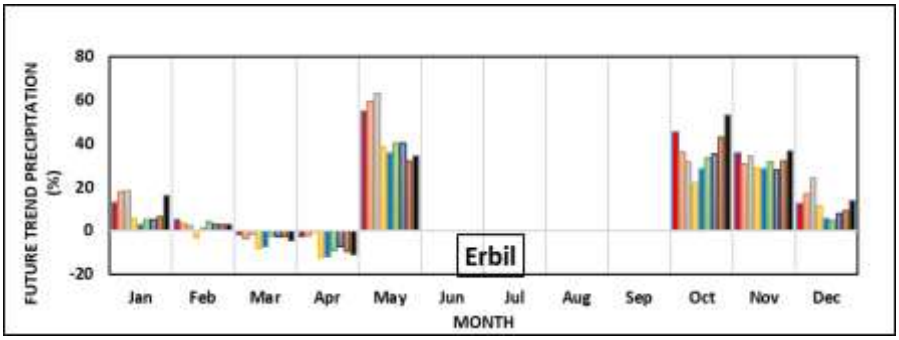
FUTURE TREND PRECIPITATION (%)
Erbil
MONTH
Jan Feb Mar Apr May Jun Jul Aug Sep Oct Nov Dec

Journal of Ecohumanism
2024
Volume: 3, No: 8, pp. 2207 – 2234
ISSN: 2752-6798 (Print) | ISSN 2752-6801 (Online)
https://ecohumanism.co.uk/joe/ecohumanism
DOI: https://doi.org/10.62754/joe.v3i8.4898

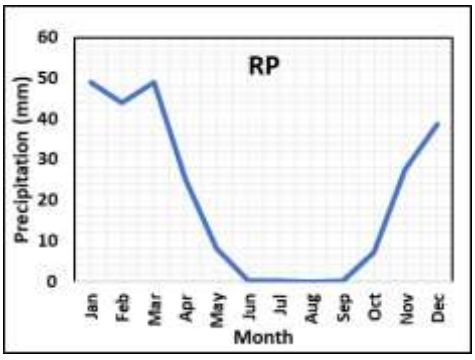

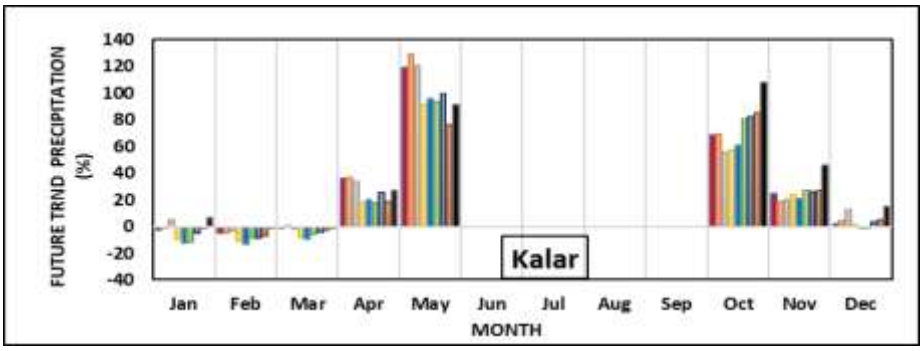

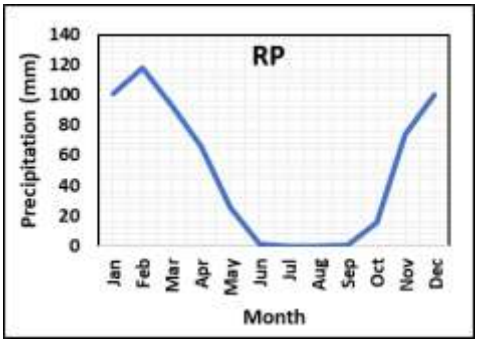

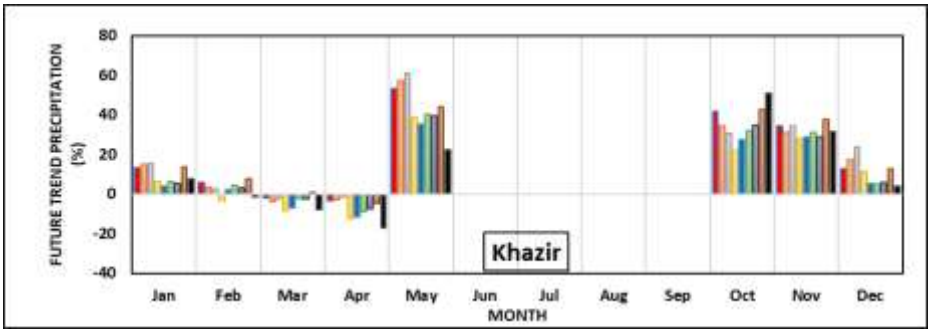

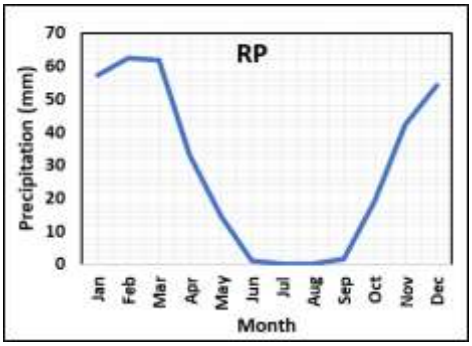

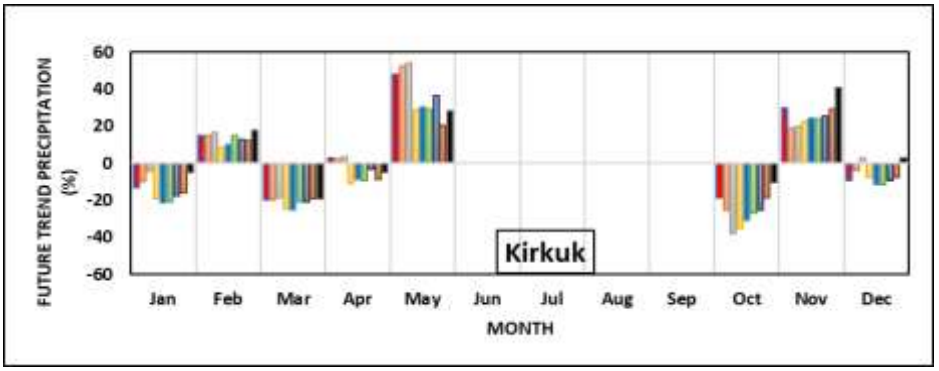

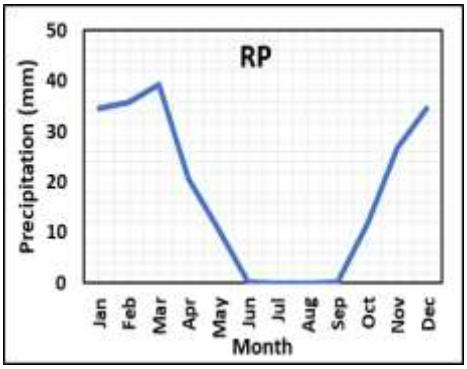

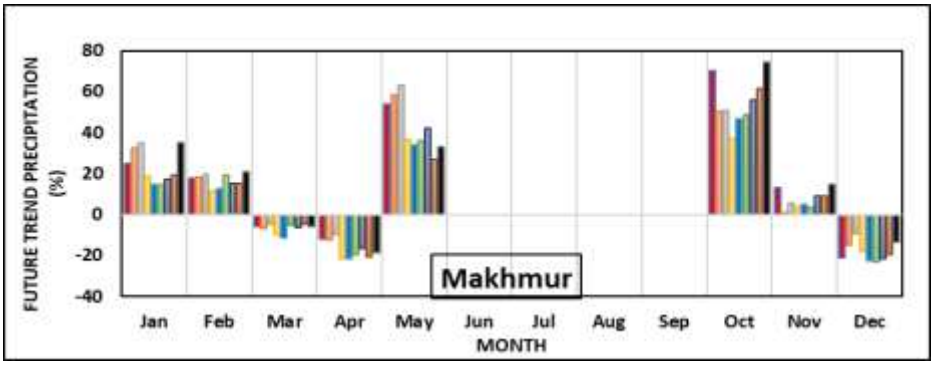

Journal of Ecohumanism
2024
Volume: 3, No: 8, pp. 2207 – 2234
ISSN: 2752-6798 (Print) | ISSN 2752-6801 (Online)
https://ecohumanism.co.uk/joe/ecohumanism
DOI: https://doi.org/10.62754/joe.v3i8.4898

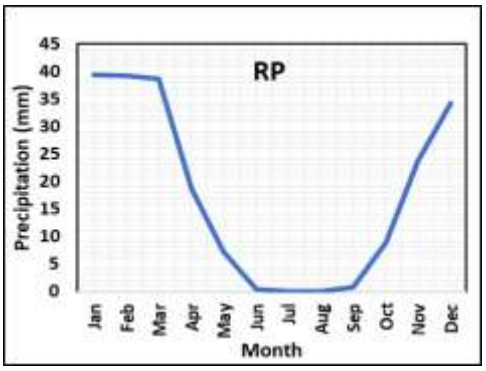

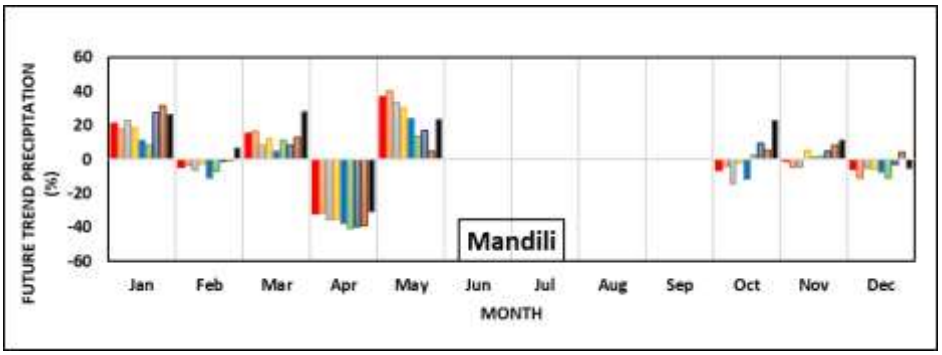

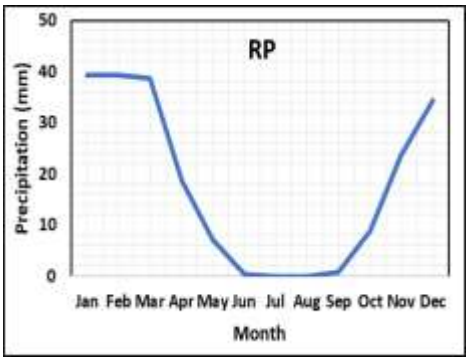

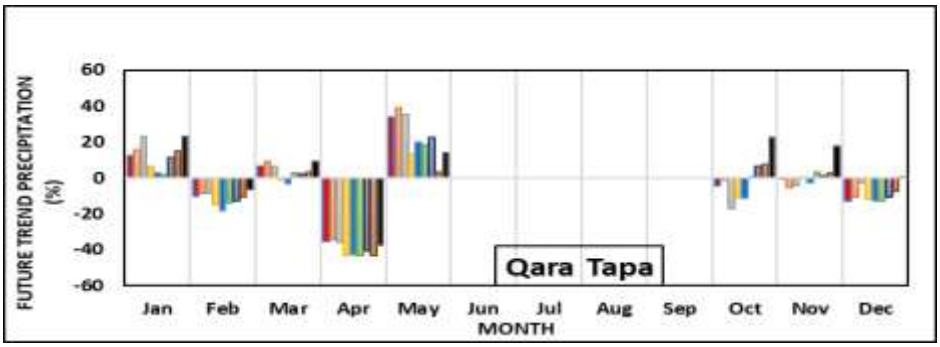

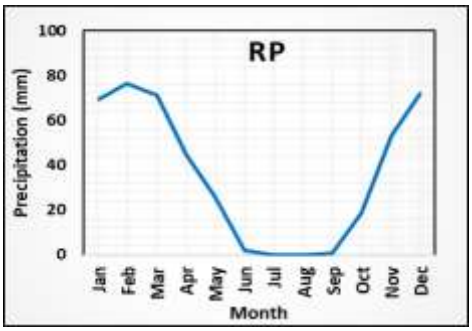

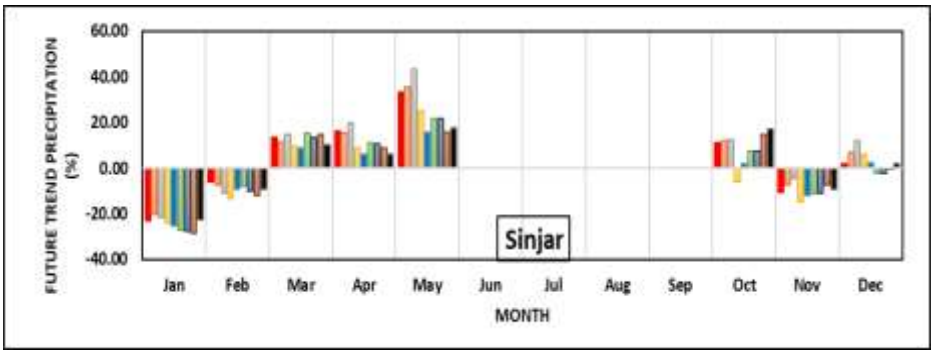

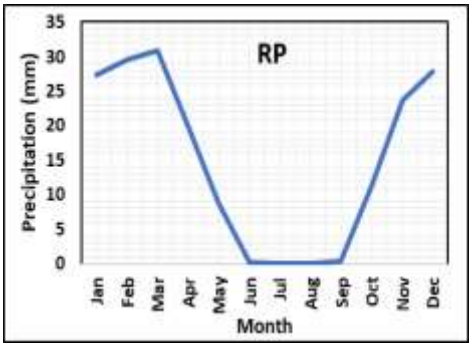

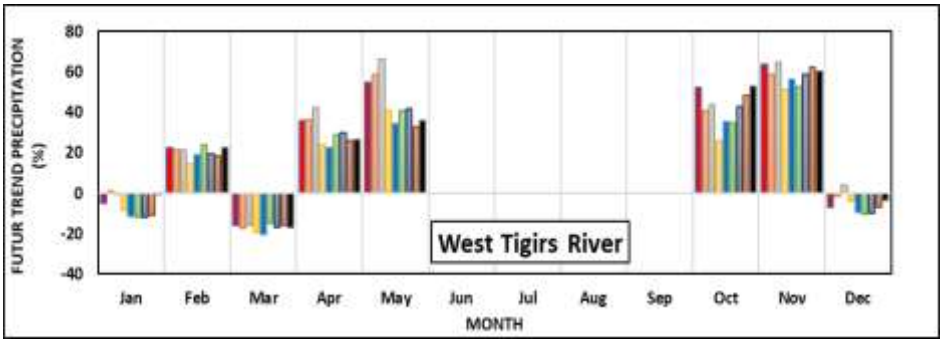

Journal of Ecohumanism
2024
Volume: 3, No: 8, pp. 2207 – 2234
ISSN: 2752-6798 (Print) | ISSN 2752-6801 (Online)
https://ecohumanism.co.uk/joe/ecohumanism
DOI: https://doi.org/10.62754/joe.v3i8.4898

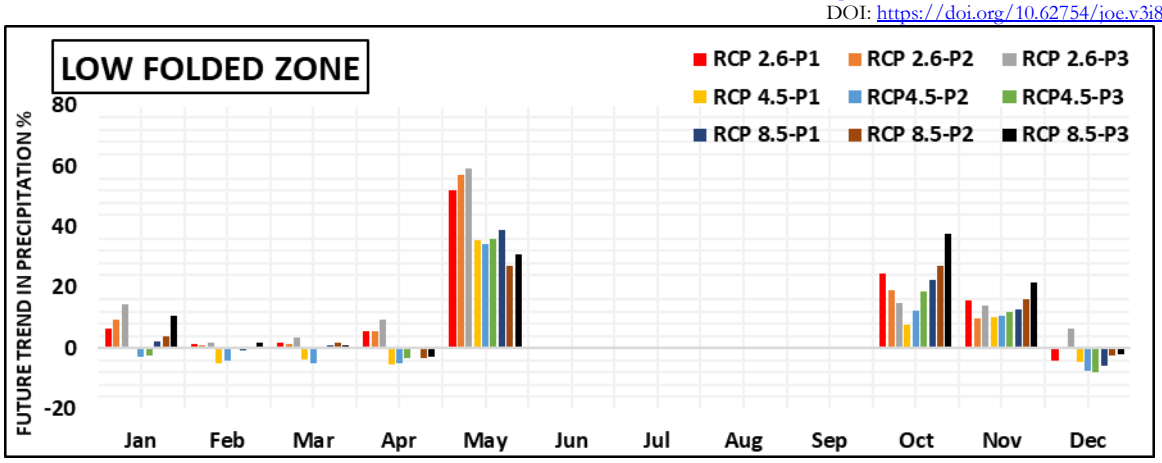

Fig.9. The Precipitation in Reference Period and Future Trend In 13 Stations and Low Folded Zone

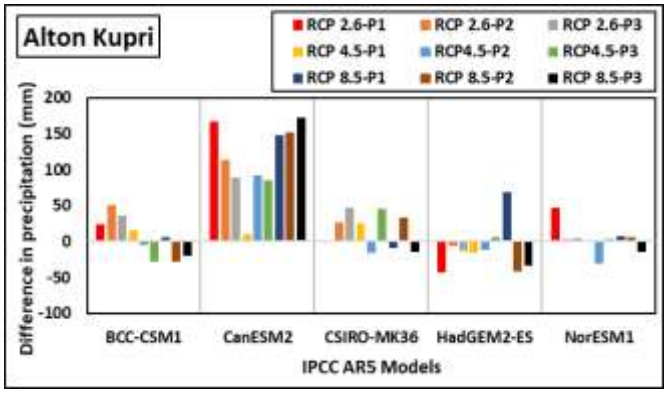

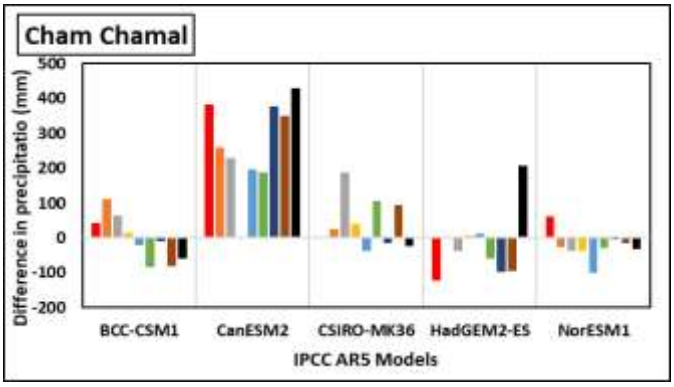

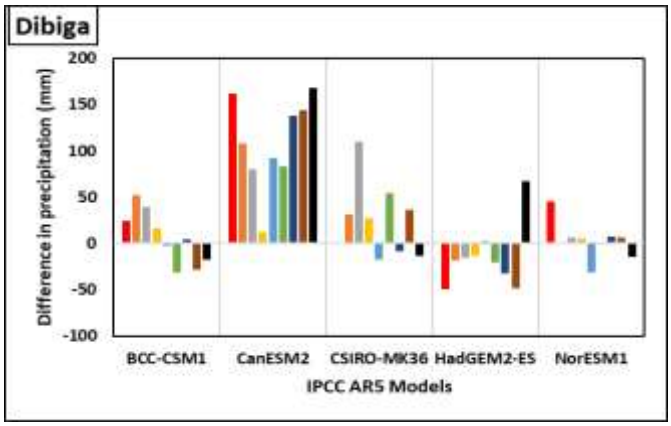

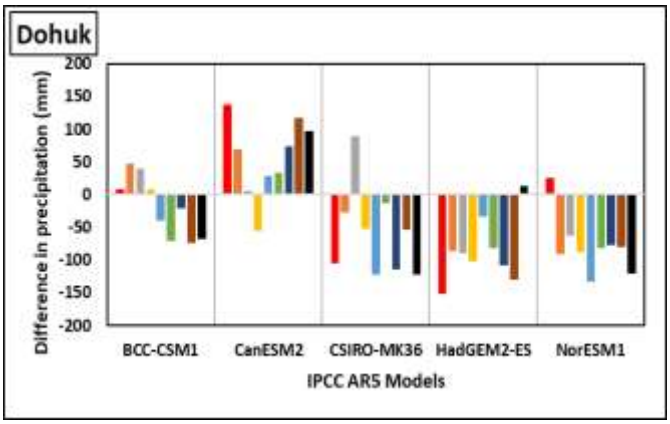

Journal of Ecohumanism
2024
Volume: 3, No: 8, pp. 2207 – 2234
ISSN: 2752-6798 (Print) | ISSN 2752-6801 (Online)
https://ecohumanism.co.uk/joe/ecohumanism
DOI: https://doi.org/10.62754/joe.v3i8.4898

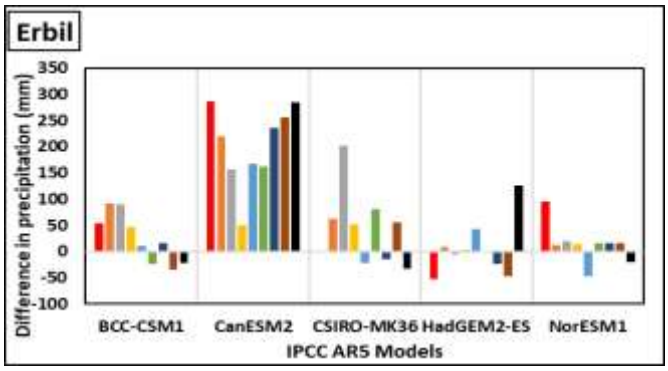

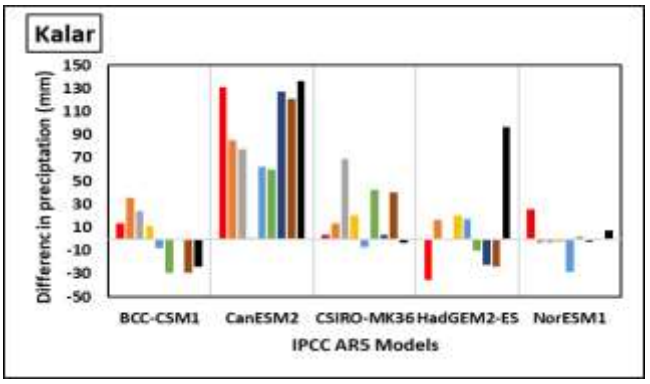

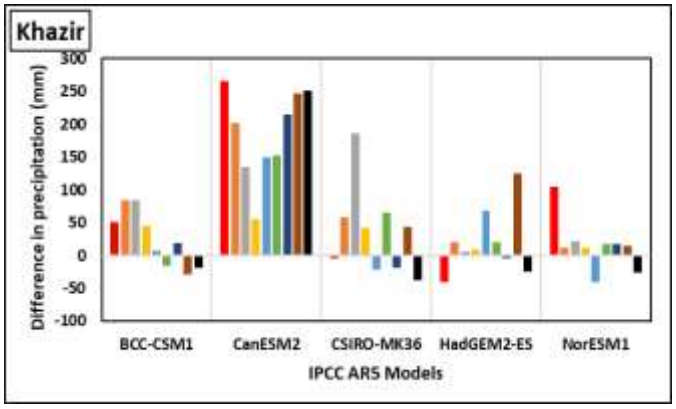

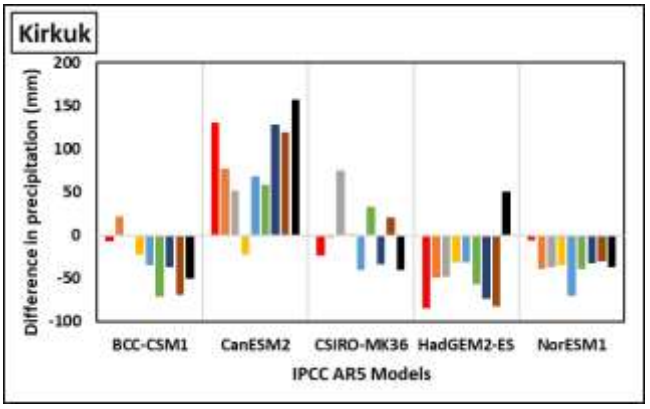

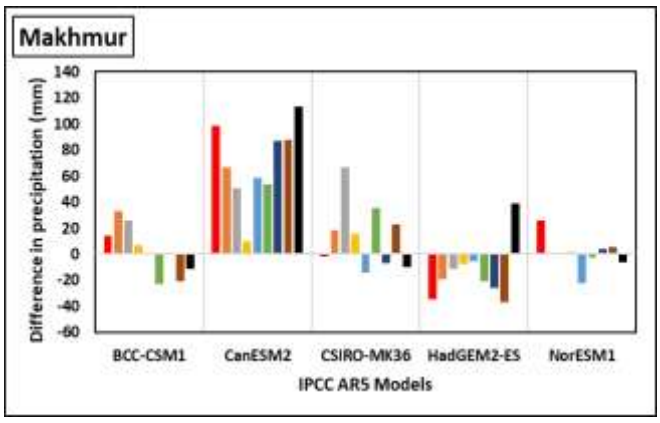

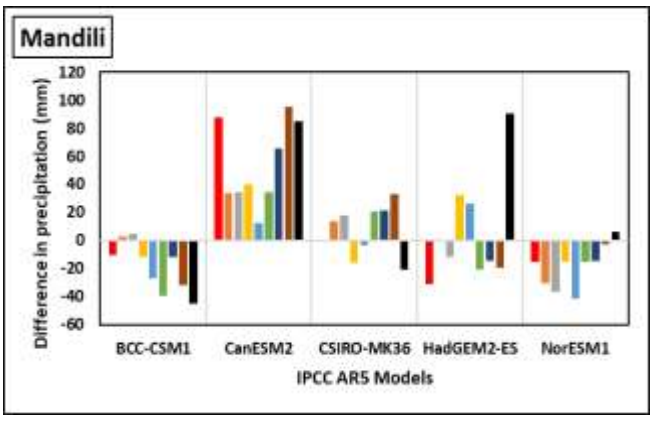

Journal of Ecohumanism
2024
Volume: 3, No: 8, pp. 2207 – 2234
ISSN: 2752-6798 (Print) | ISSN 2752-6801 (Online)
https://ecohumanism.co.uk/joe/ecohumanism
DOI: https://doi.org/10.62754/joe.v3i8.4898

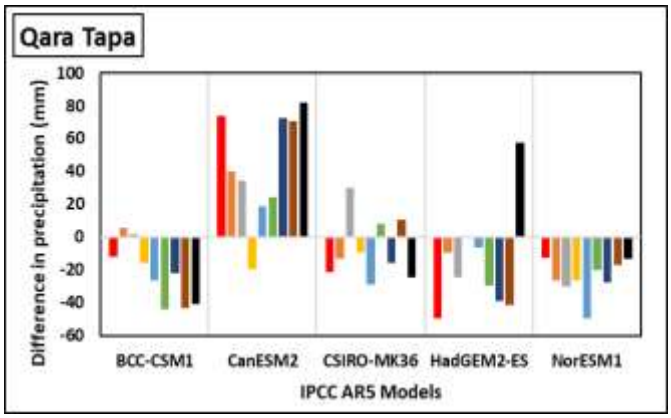

Fig. 10 Annual Precipitation Differences Between Future and Observed Periods

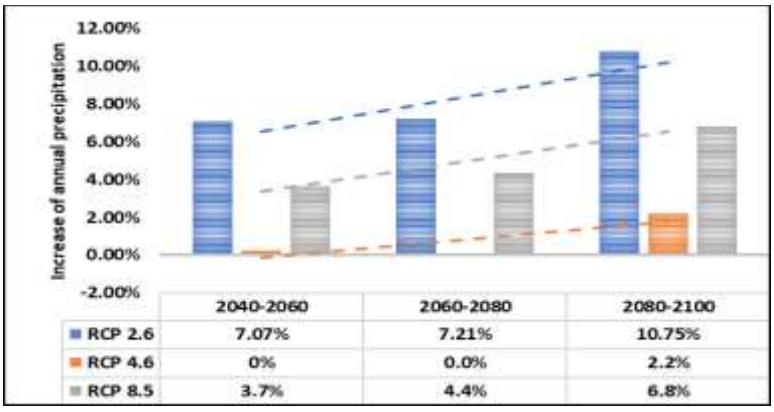

Fig. 11 Percentage of Average Annual Precipitation Increases for Low Folded Zone

Discussion

Based on the statistical analysis results, the model LARS-WG demonstrates a reasonable level of accuracy in generating temperature and precipitation projections for the study area, thus enabling reliable weather forecasting in the future ؟ The results indicate a projected temperature increase for the selected field stations during the twenty-first century, with an average range of 1.88 to 5.84 degrees Celsius. The variation in the projected temperature increase can be attributed to the differences in the scenarios used. However, it is important to note that the downscaling process introduces some uncertainty to the projected results. The overall findings are consistent with previous research conducted in Iraq, as indicated by various studies [15, 40, 38, 41]. These studies and current research reveal a general trend of increasing temperatures in Iraq, albeit with varying rates depending on the location. The northern regions experience a relatively smaller degree of temperature increase, while the central, western, and southern regions exhibit more pronounced rises. The projected temperature changes are expected to contribute to desertification [42], land use, and land cover changes, impacting agriculture [40], and water supplies in Iraq. The acceleration of surface water evaporation exacerbates water shortages, underscoring the need for sustainable solutions to mitigate and adapt to these consequences. Climate variations have been identified as significant factors in the growing dust and sand storms and other extreme weather events, which have recently been observed in various regions of Iraq [43, 44].

In terms of precipitation, the study reveals variable annual increases over the observed period under different emission scenarios (RCP2.6, RCP4.5, and RCP8.5). The projected increase ranges from 7.07% to 10.75% for RCP2.6, 0% to 2.2% for RCP4.5, and 3.7% to 6.8% for RCP8.5. These findings are consistent

Journal of Ecohumanism
2024
Volume: 3, No: 8, pp. 2207 – 2234
ISSN: 2752-6798 (Print) | ISSN 2752-6801 (Online)
https://ecohumanism.co.uk/joe/ecohumanism
DOI: https://doi.org/10.62754/joe.v3i8.4898

with prior research conducted by several researchers Researcher [38]. The increase in precipitation may be attributed to sporadic heavy rainfall events occurring unevenly during the rainy seasons.

While climate change is a physical process primarily driven by changes in climatic variables, it is also influenced by economic, environmental, and social factors that shape the evolution of human civilization over time. Therefore, mitigating and adapting to the effects of climate change requires proactive measures from socioeconomic groups in the study area. These measures span various fields, including long-term integrated national water resource management and planning, the rehabilitation of water treatment plant infrastructure, the utilization of alternative water resources such as recycled wastewater through the establishment of recycling water plants, rainwater harvesting techniques, investment in renewable energy sources (such as solar and wind energy) to reduce greenhouse gas emissions, and the implementation of green infrastructure strategies. These strategies aim to address the environmental impacts of climate change.

Conclusions

This study examined the climate change trends and future projections in Iraq's Low Folded Zone region. We gained valuable insights into the expected temperature and precipitation pattern changes by utilizing advanced modelling techniques and analyzing data from multiple sources. The findings revealed that temperatures are set to rise consistently across all selected stations in the Low Folded Zone. By the end of the twenty-first century, average annual maximum temperatures are projected to increase by 1.06 to 5.48°C. The high emission scenario (RCP8.5) showed the highest temperature increase. These rising temperatures will significantly affect various sectors, including human health, agriculture, and infrastructure.

We also observed variations in precipitation patterns in terms of spatial distribution and timing. The projected increase in annual precipitation ranged from 7.07% to 10.75% for one scenario, 0% to 2.2% for another, and 3.7% to 6.8% for a third scenario. It is important to consider these precipitation changes when planning for future water resources and regional agricultural practices.

The projected temperature increases and variable precipitation patterns highlight the urgent need for proactive measures to address the challenges posed by climate change in the Low Folded Zone. Decision-makers and planners should utilize these findings to develop effective strategies for adapting to and mitigating the impacts of climate change. Prioritizing water resource management and implementing sustainable agricultural practices are crucial steps towards building resilience in the face of climate change.

The results of this study provide scientific evidence to inform policy-making and long-term planning efforts aimed at mitigating climate change impacts in the region. They contribute to our understanding of the scale of climate change effects and can guide the development of strategies for sustainable development, protection of vulnerable communities, and preservation of natural resources. Collaboration and cooperation at an international level are also emphasized, as climate change impacts transcend national boundaries.

Conflict of Interest

The authors state no conflict of interest

Data Availability Statement

Most datasets generated and analyzed in this study are comprised in this submitted manuscript. The other datasets are available on reasonable request from the corresponding author with the attached information.

Statements and Declarations

Funding and/or Conflicts of interests/Competing interests. Also, I declare that the manuscript was done depending on the personal effort of the author, and there is no funding effort from any side or organization, as well as no conflict of interest with anyone related to the subject of the manuscript or any

Journal of Ecohumanism
2024
Volume: 3, No: 8, pp. 2207 – 2234
ISSN: 2752-6798 (Print) | ISSN 2752-6801 (Online)
https://ecohumanism.co.uk/joe/ecohumanism
DOI: https://doi.org/10.62754/joe.v3i8.4898

competing interest.

References

Evans JP. 21st century climate change in the Middle East. Climatic change. 2009;92(3-4):417-32.
Chen H, Guo J, Zhang Z, Xu CY. Prediction of temperature and precipitation in Sudan and South Sudan by using LARS-WG in future. Theoretical and applied climatology. 2013;113:363-75.
Pachauri RK, Allen MR, Barros VR, Broome J, Cramer W, Christ R, Church JA, Clarke L, Dahe Q, Dasgupta P, Dubash NK. Climate change 2014: synthesis report. Contribution of Working Groups I, II and III to the fifth assessment report of the Intergovernmental Panel on Climate Change. Ipcc; 2014.
Hassan WH, Nile BK, Al-Masody BA. Climate change effect on storm drainage networks by storm water management model. Environmental Engineering Research. 2017;22(4):393-400.
Stocker TF, Qin D, Plattner G-K, Tignor MMB, Allen SK, Boschung J, et al. Climate Change 2013: The Physical Science Basis. Contribution of Working Group I to the Fifth Assessment Report of IPCC the Intergovernmental Panel on Climate Change. Cambridge: Cambridge University Press; 2014.
Mohammed MH, Zwain HM, Hassan WH. Modeling the impacts of climate change and flooding on sanitary sewage system using SWMM simulation: A case study. Results in Engineering. 2021;12:100307.
Norby RJ, Luo Y. Evaluating ecosystem responses to rising atmospheric CO2 and global warming in a multi-factor world. New phytologist. 2004;162(2):281-93.
Mohsen KA, Nile BK, Hassan WH. Experimental work on improving the efficiency of storm networks using a new galley design filter bucket. IOP Conference Series: Materials Science and Engineering. 2020;671(1):012094.
Hassan WH, Nile BK, Mahdi K, Wesseling J, Ritsema C. A feasibility assessment of potential artificial recharge for increasing agricultural areas in the kerbala desert in iraq using numerical groundwater modeling. Water. 2021;13(22):3167.
Cubasch U, Meehl GA, Boer GJ, Stouffer RJ, Dix M, Noda A, Senior CA, Raper S, Yap KS. Projections of future climate change. InClimate Change 2001: The scientific basis. Contribution of WG1 to the Third Assessment Report of the IPCC (TAR) 2001 (pp. 525-582). Cambridge University Press.
Eden JM, Widmann M. Downscaling of GCM-simulated precipitation using model output statistics. Journal of Climate. 2014;27(1):312-24.
Vanuytrecht E, Raes D, Willems P, Semenov MA. Comparing climate change impacts on cereals based on CMIP3 and EU-ENSEMBLES climate scenarios. Agricultural and forest meteorology. 2014;195:12-23.
Hassan WH. Climate change projections of maximum temperatures for southwest Iraq using statistical downscaling. Climate Research. 2021;83:187-200.
Wilby RL, Troni J, Biot Y, Tedd L, Hewitson BC, Smith DM, Sutton RT. A review of climate risk information for adaptation and development planning. International Journal of Climatology: A Journal of the Royal Meteorological Society. 2009 Jul;29(9):1193-215.
Hassan WH, Khalaf RM. Optimum Groundwater use Management Models by Genetic Algorithms in Karbala Desert, Iraq. IOP Conference Series: Materials Science and Engineering. 2020;928(2):022141.
Khaliq MN. An Inventory of Methods for Estimating Climate Change-Informed Design Water Levels for Floodplain Mapping. Technical Report; 2019.
Mohammed MH, Zwain HM, Hassan WH. Modeling the quality of sewage during the leaking of stormwater surface runoff to the sanitary sewer system using SWMM: a case study. AQUA—Water Infrastructure, Ecosystems and Society. 2022;71(1):86-99.
Lee CY, Camargo SJ, Sobel AH, Tippett MK. Statistical–dynamical downscaling projections of tropical cyclone activity in a warming climate: Two diverging genesis scenarios. Journal of Climate. 2020;33(11):4815-34.
Rasheed AM. Adaptation of water sensitive urban design to climate change (Doctoral dissertation, Queensland University of Technology).
Hassan WH, Hussein HH, Alshammari MH, Jalal HK, Rasheed SE. Evaluation of gene expression programming and artificial neural networks in PyTorch for the prediction of local scour depth around a bridge pier. Results in Engineering. 2022;13:100353.
Hashmi MZ, Shamseldin AY, Melville BW. Comparison of SDSM and LARS-WG for simulation and downscaling of extreme precipitation events in a watershed. Stochastic Environmental Research and Risk Assessment. 2011;25:475-84.
Semenov MA, Barrow EM, Lars-Wg A. A stochastic weather generator for use in climate impact studies. User Man Herts UK. 2002:1-27.
Abd al rukabie JS, Hassan AS, Kadhum JH. Assessment CO2 Emission Intensity of Crude Oil Production in Iraq. IOP Conference Series: Materials Science and Engineering. 2020;928(7):072048.
Faruolo M, Genzano N, Marchese F, Pergola N. A Tailored Approach for the Global Gas Flaring Investigation by Means of Daytime Satellite Imagery. Remote Sensing. 2022 Dec 13;14(24):6319.
Hassan WH, Hussein HH, Khashan DH, Alshammari MH, Nile BK. Application of the Coupled Simulation–optimization Method for the Optimum Cut-off Design Under a Hydraulic Structure. Water Resources Management. 2022;36(12):4619-36.
Mueller A, Detges A, Pohl B, Reuter MH, Rochowski L, Volkholz J, Woertz E. Climate change, water and future cooperation and development in the Euphrates-Tigris basin. ResearchGate/Geoscience/Report. 2021 Nov.
Price, R.A. Environmental Risks in Iraq, K4D Helpdesk Report; Institute of Development Studies: Brighton, UK, 2018.
Adamo N, Al-Ansari N, Sissakian VK, Knutsson S, Laue J. Climate change: consequences on Iraq's environment. Journal of earth sciences and geotechnical engineering. 2018;8(3):43-58.

Journal of Ecohumanism
2024
Volume: 3, No: 8, pp. 2207 – 2234
ISSN: 2752-6798 (Print) | ISSN 2752-6801 (Online)
https://ecohumanism.co.uk/joe/ecohumanism
DOI: https://doi.org/10.62754/joe.v3i8.4898

Al-Jiburi HK, Al-Basrawi NH. Hydrogeology of the low folded zone. Iraqi Bulletin of Geology and Mining. 2012(5):133-57.

Muñoz Sabater, J. ERA5-Land monthly averaged data from 1950 to present. Copernicus Climate Change Service (C3S) Climate Data Store (CDS), 2019.

Funk C, Peterson P, Landsfeld M, Pedreros D, Verdin J, Shukla S, Husak G, Rowland J, Harrison L, Hoell A, Michaelsen J. The climate hazards infrared precipitation with stations—a new environmental record for monitoring extremes. Scientific data. 2015;2(1):1-21.

Saddique N, Bernhofer C, Kronenberg R, Usman M. Downscaling of CMIP5 models output by using statistical models in a data scarce mountain environment (Mangla Dam Watershed), Northern Pakistan. Asia-Pacific Journal of Atmospheric Sciences. 2019;55:719-35.

Zubaidi SL, Kot P, Hashim K, Alkhaddar R, Abdellatif M, Muhsin YR. Using LARS –WG model for prediction of temperature in Columbia City, USA. IOP Conference Series: Materials Science and Engineering. 2019;584(1):012026.

Semenov MA, Brooks RJ, Barrow EM, Richardson CW. Comparison of the WGEN and LARS-WG stochastic weather generators for diverse climates. Climate research. 1998;10(2):95-107.

Pirttioja N, Carter TR, Fronzek S, Bindi M, Hoffmann H, Palosuo T, Ruiz-Ramos M, Tao F, Trnka M, Acutis M, Asseng S. Temperature and precipitation effects on wheat yield across a European transect: a crop model ensemble analysis using impact response surfaces. Climate Research. 2015;65:87-105.

Salman SA, Shahid S, Ismail T, Ahmed K, Wang XJ. Selection of climate models for projection of spatiotemporal changes in temperature of Iraq with uncertainties. Atmospheric research. 2018;213:509-22.

Hassan WH, Hashim FS. Studying the impact of climate change on the average temperature using CanESM2 and HadCM3 modelling in Iraq. International Journal of Global Warming. 2021;24(2):131-48.

Hassan WH. Climate change impact on groundwater recharge of Umm er Radhuma unconfined aquifer Western Desert, Iraq. International Journal of Hydrology Science and Technology. 2020;10(4):392-412.

Eulewi HK. The phenomenon of desertification in Iraq and its environmental impacts on middle and southern Iraq, Babil Governorate, as a model. IOP Conference Series: Earth and Environmental Science. 2021;722(1):012020.

Osman Y, Al-Ansari N, Abdellatif M. Climate change model as a decision support tool for water resources management in northern Iraq: a case study of Greater Zab River. Journal of Water and Climate Change. 2019;10(1):197-209.

Faqe Ibrahim GR. Urban land use land cover changes and their effect on land surface temperature: Case study using Dohuk City in the Kurdistan Region of Iraq. Climate. 2017;5(1):13.

Sissakian V, Al-Ansari N, Knutsson S. Sand and dust storm events in Iraq. Journal of Natural Science. 2013;5(10):1084-94.

Valavanidis A. Extreme weather events exacerbated by the global impact of climate change. Available online: Chem-toxecotox. org/ScientificReviews (accessed on 28 May 2023). 2022.

Jabbar MA, Hassan AS. The Daily Pattern at 500 hPa Geopotential Heights and Its Association with Heavy Rainfall over Iraq. Iraqi Journal of Science. 2023:1498-507.

Al-Waeli LK, Sahib JH, Abbas HA. ANN-based model to predict groundwater salinity: A case study of West Najaf–Kerbala region. Open Engineering. 2022;12(1):120-8.

Al-Rawabdeh A, Al-Ansari N, Al-Taani A, Al- Khateeb F, Knutsson S. Modeling the risk of ground- water contamination using modified DRASTIC and GIS in Amman-Zerqa Basin, Jordan. Open Engineer- ing. 2014;4(3):264-80.